UNIVERSITY OF OKLAHOMA

GRADUATE COLLEGE

FINITE ELEMENT MODELING OF RESIDUAL MECHANICAL HEARING FUNCTION AFTER COCHLEAR IMPLANT SURGERY

A THESIS

SUBMITTED TO THE GRADUATE FACULTY

in partial fulfillment of the requirements for the

Degree of

MASTER OF SCIENCE

By

NICHOLAS CASTLE
Norman, Oklahoma
2023

FINITE ELEMENT MODELING OF RESIDUAL MECHANICAL HEARING FUNCTION AFTER COCHLEAR IMPLANT SURGERY

A THESIS APPROVED FOR THE
SCHOOL OF AEROSPACE AND MECHANICAL ENGINEERING

BY THE COMMITTEE CONSISTING OF

Dr. Chenkai Dai, Chair

Dr. James Baldwin

Dr. Fengchyuan Lai

Acknowledgements

I would like to thank my advisor, Dr. Chenkai Dai, for all his help throughout my college career, both in and out of my work in the Hearing & Balance lab. He has taught me most of what I know about the field of biomedical engineering, provided valuable help in writing this thesis, and has been an inspiration which drove me to continue my education beyond my bachelors degree. He has always had a profound belief in my abilities even when I struggled early on to begin my work on the models described here. Dr. James Baldwin has been another inspiration for me, especially in teaching me the finite element method which I have developed a strong passion for. I thank Dr. Fengchyuan Lai for his participation as a member of my committee and for the excellent teaching he provided me in his classroom. I would also like to extend a special thanks to the two leading undergraduate research assistants in our lab, Cayman Matson and Brett Petersen, for their effort in the creation of the rhesus model in this paper, as well as their hard work on the other projects we have worked on together in my time here. They have all made my career at The University of Oklahoma more valuable and I hope to stay in touch with them long into the future. I also appreciate the support of my family and partner throughout my college career. Their encouragement was a driving force for my work, which would not have been possible without them.

Abstract

Cochlear implant (CI) surgery is one of the most utilized treatments for severe hearing loss. Though CI surgery is proven to improve patients' quality of life, results are variable as damage to very delicate inner ear tissues can be difficult to avoid. However, even the effects of optimal scala tympani insertions on the mechanics of hearing are not yet fully understood. This project presents two finite element models of the inner ear to study the interrelationship between the mechanical function of the cochlea and the insertion of a cochlear implant electrode, one derived from the chinchilla inner ear and one derived from the rhesus monkey inner ear. These subjects were chosen due to their wide usage in inner ear research as designs of the typical device tend to progress from chinchilla animal studies, to rhesus animal studies, and finally to human trials. Both FE models include a three-chambered cochlea and full vestibular system, rarely seen in prior studies. The procedure used to create these models is low-cost, rapid, and reproducible, and results in a highly detailed model using μMRI imaging as the data source.

In the chinchilla model's unimplanted state, data indicative of the tuning effect of the cochlea closely matched results obtained in In Vivo studies. In its implanted state, the chinchilla model found minimal loss of residual hearing or alteration of the cochlea's tuning effect regardless of CI insertion angle. Its results suggest that an emphasis should be put on developing CI's with maximal insertion angles and minimal trauma during insertion. The more detailed rhesus model is presented with its preliminary results and plans for its continued development. In the future, both models can be reused with minimal alteration to study a broad range of phenomena such as vestibulo-cochlear interaction, the results of vestibular implant surgery, and the effects of various pathologies on hearing function.

Table of Contents

List of Figures

List of Tables

1 Introduction

1.1 Hearing Loss

1.1.1 Prevalence

Hearing loss is a global public health issue that is often underestimated. More than 20% of the global population has some form of hearing loss, amounting to over 1.5 billion people [35]. Of this population, over 430 million have disabling hearing loss. 34 million children have some amount of hearing loss. In 60% of these cases the cause was preventable. Hearing loss is an 'invisible disability'; most policy-makers do not adequately address it and many individuals do not seek treatment until hearing loss has become severe or profound [80]. Exact guidelines vary from study to study but, according to the WHO, sounds even as loud as the average doorbell (80dB) are capable of causing hearing loss over extended periods of time (40 hours). Individuals can be safely exposed to 100 dB, about the volume of a hair dryer, for only 20 minutes a week. Concerts, one of the largest causes for concern, often reach volumes upwards of 100 dB or even 110 dB. These volumes can cause hearing loss in less than 10 minutes [141]. The strongest government guidelines limit volumes without hearing protection to below 80 dB, in most settings. When these guidelines are incorporated into policy tangible benefits are felt. Therefore, the best solution to hearing loss is to avoid it in the first place with strong regulation. It is clear that hearing loss is a very large problem globally. When considering the global population, more than 5% suffer from disabling hearing loss [29]. Today, that amounts to around 395 million people.

In the United States, the greatest factor affecting prevalence of hearing loss is age [29]. A 2016 analysis by Dr. Goman and Dr. Lin of Johns Hopkins found

that more than 20% of Americans 12 years or older have some form of hearing loss [51] . Only around 2.5% of individuals age 12-19 have hearing loss, increasing to 16.04% for individuals in their 40's, 33.74% in their 50's, and 48.92% in their 60's. By the time an individual is 70 or older nearly 75% exhibit hearing loss in at least one ear. In sum, over 60 million Americans exhibit some form of hearing loss. These numbers drop when only considering severe to profound hearing loss, where medical intervention is most important. Around 2.5% of Americans aged 12 years or older exhibit severe to profound hearing loss in at least one ear. This ranges from nearly 0% in the lowest age group, mostly originating from congenital defects, to around 2% of individuals in their 50's and nearly 7% of individuals in their 70's or above. In total, 6-7 million Americans had severe to profound hearing loss in at least one ear when examining data from 2001 to 2010. These numbers are especially disturbing as hearing loss is associated with other negative social and health outcomes. These include declining cognitive performance, higher incidence of dementia, and social isolation [30]. When it comes to the relationship between hearing loss and cognitive decline, two primary hypotheses exist. The first is that cognitive decline and reduced hearing function share a common cause. The second is that hearing loss is a direct contributor to cognitive decline. The latter is called the cascade hypothesis and is supported by data indicating that the use of hearing aids improves cognition beyond what would be expected of increased hearing function. This result can be extrapolated to the use of cochlear implants; methods which improve hearing function have significant effects on cognition, and therefore reduction in the incidence of dementia in older patients [110].

1.1.2 Common Causes

Many diseases which affect hearing or balance often have some effect on the other. This is because the cochlea and vestibular system are connected directly with lymphatic fluid which fills the entirety of the inner ear. Examples of such diseases include Ménière's disease, otitis media, and otosclerosis. Each of these diseases have different mechanisms.

Sensorineural hearing loss Sensorineural hearing loss is caused by the death of inner ear hair cells. This causes higher pitches of sound to become muffled, makes it harder to differentiate between different pitches, and generally decreases an individuals hearing function. Age is the most common cause of this type of hearing loss. Exposure to loud noise, certain diseases, drugs, and congenital abnormalities can also cause sensorineural hearing loss. Sensorineural hearing loss can effect residual hearing after cochlear implantation as well.

Ménière's disease Ménière's disease is the result of endolymphatic hydrops, a distention of the membranes in the inner ear due to increased pressure. Endolymphatic hydrops is diagnosed by examining the size of the saccule in relation to the utricle and the volume of perilymph visible in medical scans. Though its mechanism is not thoroughly understood, it is thought to stem from constrictions of blood vessels, drainage issues in the ear structure, infections, head trauma, genetics, or some combination of these factors. Despite the general lack of understanding of this disorder, there are some procedures which should be explored other than cochlear implantation. Examples include steroid injections and endolymphatic sac decompression surgery. In some cases even cochlear implant surgery (CIS) is insufficient and a complete labyrinthectomy must be performed.

Chronic otitis media Otitis media is an infection or inflammation of the middle ear which also effects the inner ear. In rare cases this can lead to permanent hearing loss which necessitates CIS. However, this should never be used as the first option for treatment. Patients should be evaluated for the viability of tympanoplasty with mastoidectomy. This procedure removes diseased cells from the inner ear and repairs perforations which may be present in the tympanic membrane.

Otosclerosis Otosclerosis is the fusing of the stapes to other bones located in the middle or inner ear. This often results in reduced, or complete loss of, hearing function as sound waves cannot propagate to the sensory organs in the inner ear. In many cases stapedectomy is the preferred solution, where the stapes is removed and a prosthesis is installed in its place. However, in the worst cases of otosclerosis where the oval window membrane is compromised CIS can be most effective and prove a life-changing treatment.

1.2 Inner Ear Anatomy

The ear is generally organized into the outer, middle, and inner ear. The outer ear is what is visible to outside observers. The outer ear consists of the pinna, the external auditory canal, and the tympanic membrane [20]. The middle ear contains the auditory ossicles which transmit vibrations from the tympanic membrane to the inner ear through an air-filled space. The inner ear is the most important part of the ear as it provides the senses of hearing and balance. It is located within the bony labyrinth of the temporal bone and consists of two distinct but connected systems, the cochlea and the vestibular system. In this work I will focus my attention on the inner ear.

1.2.1 Cochlea

The cochlea is responsible for hearing and takes the general shape of a nautilus shell. The cochleas spiral structure and unique material properties allow resonance with different frequencies at set locations along its length, creating a tonotopic map where displacement of different positions in the cochlea correspond to specific frequencies perceived by the brain. This capability is known as the tuning effect of the cochlea. Each species has a different frequency-position function which models these locations of resonance, a very useful tool for comparing hearing function between species and in the creation of hearing devices. These functions are detailed in Greenwood's work on the subject [53].

The cochlea consists of three chambers, the scala vestibuli, the scala media, and the scala tympani. The scala vestibuli and tympani are filled with perilymphatic fluid and are directly connected through the helicotrema, an opening in the osseous spiral lamina at the apex of the cochlea. The helicotrema is typically modeled as the space between the cochlear duct and the bony labyrinth at the cochlea's apex. In actuality, the cochlear duct extends fully to meet the bony canal with the helicotrema lying medial to the apex of the cochlea. This structure varies in size between individuals and is believed to influence low-frequency hearing via changes to the pressure differential across the cochlear partition [134]. The scala media is a separate fluid volume, filled with endolymph. All vibrations between the endolymph and perilymph must therefore travel through the membranes of the scala media, the most important of which are the Reissner's Membrane and basilar membrane (BM). The Reissner's Membrane (RM) separates the scala media from the scala vestibuli while the basilar membrane separates the scala media from the scala tympani.

In function, sound waves are transmitted from the tympanic membrane, or eardrum, through the auditory ossicles and into the oval window membrane of the inner ear. The stapedial annular ligament is the elastic boundary between the stapes footplate and the bony wall of the oval window membrane [42]. Vibrations are transmitted from the oval window membrane (OWM) into the perilymph of the cochlea to the scala vestibuli where they propagate through the cochlea's length. At the apex of the cochlea, vibrations travel through the helicotrema into the scala tympani, then travel back to the base of the cochlea. Waves are dissipated at the round window membrane [1]. The scala media, being situated between the scala vestibuli and tympani, senses vibrations using hair cells within the organ of Corti, displaced as a function of the material properties and dimensions of the basilar membrane. Ultimately, the properties and geometry of the basilar membrane are the primary factors that influence the cochlea's tonotopic map. Electrical signals from these hair cells transmit to the spiral ganglion, through the auditory nerve, and finally to the brain where they are processed and provide the sense of hearing. In this work the displacement of the basilar membrane is examined as an approximation for displacement of the organ of Corti, given its comparatively simple structure and importance to the tuning effect of the cochlea.

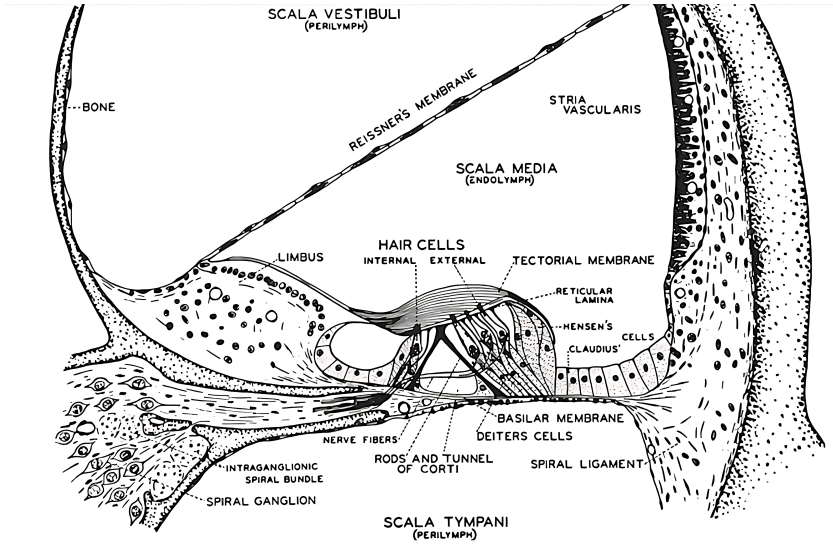

Figure 1: Basic anatomy of the cochlear duct. Adapted from the book Auditory System, a part of the Handbook of Sensory Physiology book series, with the permission of Springer Nature. [1]

Healthy cochleas come in many different shapes and sizes, even among a single species. In humans the length of a healthy cochlea is around of 35.58 mm with a standard deviation of 1.41 mm [68]. The lengths vary greatly in cochleas that are malformed due to congenital defects, but are typically much shorter than cochleas which are not deformed. This length is an important consideration when choosing the model of cochlear electrode to be used; too long of an electrode will likely cause cochlear trauma and too short of an electrode will have sub-optimal results, being unable to stimulate the desired length of the spiral ganglion.

1.2.2 Vestibular System

The vestibular system is formed by a series of connected chambers and canals which act as an organic gyroscope [70]. The semicircular canals, equipped with their sensory organs, the cupulae, allow sensation of angular acceleration due to

their curved shape. Lymphatic fluid flows through the semicircular canals as a result of angular acceleration of the head, bending the cupulae and the sensory hair cells contained within them, sending electrical signals to the brain. Otoliths, hard calcium carbonate structures, are used to detect the linear acceleration of the head. Otolith organs include the saccule and utricle, with the majority of their sensory hair cells contained in the saccular macula and the utricular macula. The saccular macula detects vertical acceleration while the utricular macula detects horizontal acceleration. The anatomy and function of the vestibular system is displayed in Figure 2.

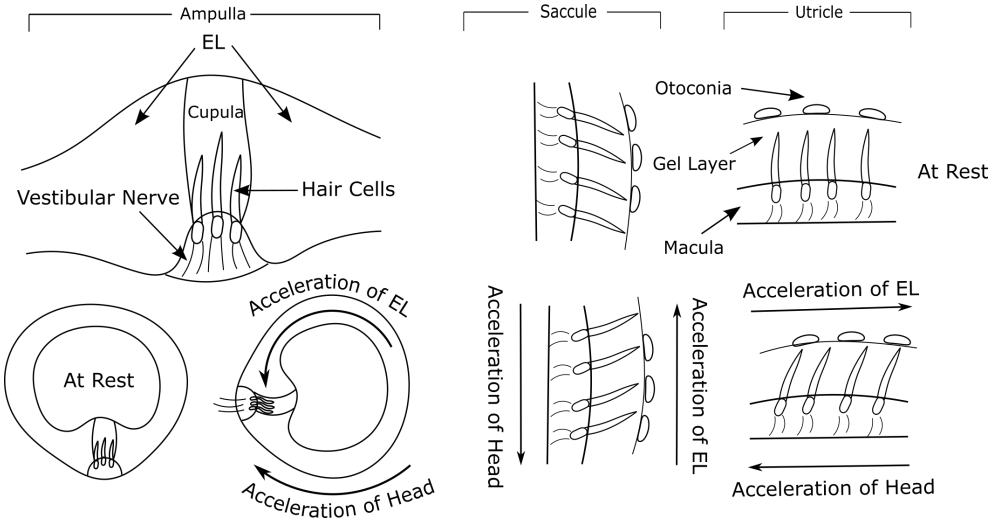

Figure 2: Basic anatomy and function of the vestibular system at rest and under acceleration.

The vestibular system is intimately connected to the movement of the eyes. The vestibular system is used by the brain to allow smooth movement of the eyes, known as the vestibulo-ocular reflex (VOR). The angular and linear accelerations detected by the vestibular system directly influence stability of the retina by informing eye movements opposite to the direction of acceleration. VOR also influences

posture and gait. In severe cases of impairment, patients have trouble standing and walking, inhibiting their ability to perform simple tasks. The importance of the vestibular system cannot be understated as the loss of its vestibular function can be a debilitating condition. It is estimated that approximately 35% of the population aged 40 years or above experience some form of vestibular problem [2]. Because the vestibular system is directly connected to the cochlea [67], including it in the two models described in this work was necessary. The extent of their interrelationship is not yet fully comprehended, thus, it was deemed prudent to incorporate the vestibular system in both models.

1.3 Cochlear Implants

1.3.1 Clinical Significance

In cases where hearing aids are no longer useful or sufficient, cochlear implant (CI) surgery is the standard procedure for the treatment of severe hearing loss. CIS has been approved by the FDA since 1996 for use in adults and since 1997 for use in children. Modern CI surgery often significantly improves patients' health-associated quality of life [59, 66, 84, 92, 117]. Children can develop age-appropriate speech skills [47, 88] and adults can regain open-set speech recognition [48].

1.3.2 Design and Function

Cochlear implants are prostheses which are a functional replacement for electrical stimuli from hair cells in the cochlea [72]. Cochlear implants have several components which work together to convert sound received by an external microphone to sensible electrical signals transmitted to the auditory nerve [91]. The microphone, typically worn behind the ear like a hearing aid, is used to detect sound. The infor-

mation from the microphone is processed by an external speech processor and the resultant information is sent to a transmitter. This transmitter is external to the body and sends electrical signals to a receiver implanted in a hollow cavity created in the bone behind the ear. This receiver sends the impulses from the transmitter to the electrode array. The general position of these components is seen in Figure 3.

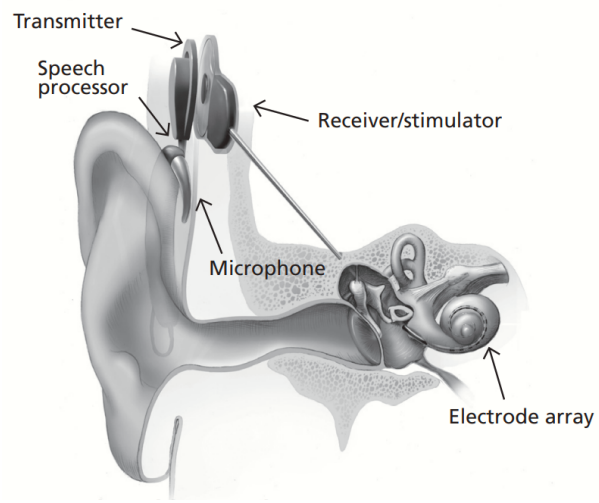

Figure 3: Major components of a cochlear implant. Adapted from a figure produced by the NIH/NIDCD available online on their web page titled Cochlear Implants [91].

The surgical procedure for cochlear implantation involves an incision behind the ear, through which the auditory canal and labyrinthine block containing the three semicircular canals are exposed. [72]. A section of the temporal bone is hollowed out to create a bone bed for the receiver of the implant. Then, a canal is drilled through the bone bed into the middle ear where the round window membrane (RWM) can be accessed. A small nerve responsible for taste, the chorda tympani, may need to be displaced during this process especially in young patients where

tolerances are smaller. Surgeons must take special care to avoid damaging this nerve and may monitor the facial nerve during surgery as an extra precaution. The receiver is implanted into the bone bed and the cochlear electrode carrier positioned to prepare for insertion through the RWM. The RWM is completely exposed through removal of bone around the cochlea, a small incision made, and the electrode carrier slowly and carefully inserted through the drilled canal of the bone and into the RWM. This step varies depending on the variety of electrode chosen but the goal is always to minimize cochlear trauma. The final step is closure of the cochlea, where muscle or fascia are used to plug any gaps, and wound closure of the incision in the head.

There are many different designs of CI electrodes with variable lengths, stiffnesses, and procedures for implantation [34]. Electrodes are either straight or pre-curved [54]. Straight electrodes are positioned near the lateral wall of the scala media, while pre-curved electrodes are positioned as close to spiral ganglion cells as possible. The spiral ganglion is the nerve attached to the hair cells of the cochlea and is therefore the target of electrical stimulation. Straight electrodes are designed to be as flexible as possible to avoid trauma to soft tissues, inserted such that they naturally curve as they contact to lateral wall of the cochlea, while pre-curved electrodes utilize specialized stylets or sheaths to insert the electrode without trauma. Straight electrode arrays are the most common and easiest to implant.

One of the leading manufacturers of CI's is MED-EL. MED-EL's most popular CI electrodes are straight electrodes, specifically their FLEX and STANDARD series of electrodes [34]. These are touted as the companies "softest and most flexible electrode arrays designed for the majority of patients and optimised for Structure

Preservation and the preservation of residual hearing." [85] These electrodes vary in length from 20 mm to 31.5 mm, corresponding to different insertion angles. Insertion angles are the angle which the cochlear implant travels through the length of the cochlea. For example, full insertion through the first twist would be a 360° insertion angle, through the second would be a 720° insertion angle, and so on.

Generally, the materials used in cochlear implants include silicone, platinum, titanium, and ceramics [118]. The electrode array uses platinum for the electrode contacts and for the wires internal to the electrode array. Silicon is used as the main body of the array. Titanium or ceramics are typically used for the sealed housing of the receiver embedded in the skull. All these materials are regarded as having good biostability. The flexibility of silicon makes it ideal for the electrode array as flexibility is vital to avoiding trauma during electrode insertion. Platinum is good for wires and contacts owing to its low reactivity and resistance to corrosion. Titanium is light, inert, and very strong, making it a suitable choice for the housing. Ceramics are easy to embed wires in while maintaining a good seal, but are more prone to fracture under high stress. Because of the brittleness of ceramics, in most cases titanium is used as the main housing for the receiver and ceramics are reserved for sealing the point where wires exit. Ceramics are still viable as a material for the main housing; however, they have been known to break after physical trauma.

Some candidates for CI surgery have congenitally malformed cochleas, accounting for approximately 20% of congenital hearing loss cases [112]. In these cases, special electrode arrays are necessary to prevent leakage of fluids and account for irregular cochlear lengths. MED-EL offers their FORM series of electrodes specifically for this purpose. According to MED-EL they are, "designed specifically for

malformed cochleae and for instances where leakage of cerebrospinal fluid (CSF) is expected. Each FORM array features an integrated SEAL designed to close off the cochlear opening making it easier for surgeons to apply additional tissue for sealing the area once the electrode array has been inserted." [85]

CI electrodes are designed with a series of contacts spaced along the length of the cochlea. Physiological differences in each patient necessitates the ability to program the response of the implant on a patient-by-patient basis [120]. CI's are programmed for each patient dependant on their response to stimulation by the CI electrode. This is can be done subjectively, using the patients input as a guide. The patient can be asked what minimum and maximum stimulation levels from the implant are comfortable to optimize results. However, it is also possible to use electrically evoked compound action potentials (eCAPs) data to inform programming where the patient is unable to provide adequate input, often the case with young children and infants [57,125]. eCAPs are measures of the auditory nerve's response to electrical stimulation which can be obtained by sending out a signal from a contact on the implanted electrode and monitoring the voltage in the surrounding area of the cochlea. Using this data the minimum and maximum stimulation levels of the implant can be determined without patient input. This is an essential part of CI fitting and all manufacturers include integrated tools to measure eCAP response.

1.4 Residual Hearing

Residual hearing is defined as the residual, natural function of the inner ear after cochlear implantation. Many patients who choose cochlear implantation as their solution to hearing loss retain some amount of hearing function, even if it may not

be entirely evident to the patient. The leading cause of residual hearing loss during CI surgery is loss of mechanical function of the inner ear, though damage to the auditory nerve efferents can be more debilitating and difficult to treat effectively [133]. Residual hearing is an important part of patient outcomes after CI surgery. It contributes to the long-term efficacy of CI's, especially in the spatial recognition of sound in the users environment [121, 132]. Residual hearing is also a major contributor to the recognition of low and high frequency sounds, as well as hearing under challenging conditions, such as in a busy restaurant with competing speech. Residual hearing is especially important for bimodal CI users, with a CI in both ears, as all the aforementioned problems with spatial and low-frequency recognition are magnified [37]. Generally, bimodal CI users tend to have significantly worse outcomes than contralateral CI users [49]. Without binaural hearing of low-to-mid frequency sounds patients struggle to identify the origin of sounds. However, patients are able to partially compensate for low residual hearing as they adapt to their CI. Usually, this occurs after a significant amount of time has passed since implantation.

1.4.1 Cochlear trauma

Most sources report that the magnitude of CI surgery's effect on residual hearing is largely dependent upon whether cochlear trauma takes place during CI surgery. Trauma is usually attributed to the dislocation of the CI electrode from the scala media or vestibuli [131]. Dislocation can arise due to a variety of factors, thus necessitating the correct choice of an electrode, the surgical technique, and the insertion angle [18]. An important consideration is the morphology of the patient's cochlea, as shorter and smaller cochleae tend to have higher rates of intracochlear

dislocation when electrodes are fully inserted [69]. In most modern cases, CI electrodes are correctly placed in the scala tympani with minimal trauma. When inserted using a cochleostomy, where a hole is drilled elsewhere in the cochlea, there is a higher chance of significant cochlear trauma. As a result, RWM insertion is the preferred method [135]. Understanding the effects of typical CI electrode placement on the finer sensitivity of the BM is an important step toward further improvement of CI electrode design. The two FE models in this work assume completely atraumatic insertion of the CI electrode. This assumption makes these FE models a good analog for what is possible in the future of CI development.

1.4.2 Scar Tissue

Stiffening of the round window membrane is a common occurrence after cochlear implantation, particularly when the CI electrode is inserted into the scala tympani [78]. Following implantation, the round window membrane must heal around the electrode, leading to the formation of scar tissues. This causes the membrane to thicken and alters its material properties [46]. Since the round window membrane is responsible for the release of excess energy, its alterations can significantly affect hearing sensation [78].

1.4.3 Insertion Angle

Insertion angle is a major contributor to CI effectiveness [94]. When longer electrode models are selected, typically with an angle of insertion greater than 540 degrees, lower frequencies become more perceptible to patients. Music becomes more enjoyable, and the quality of life increases compared to those patients with shorter CI electrodes [107]. In cases where CI surgery results in minimal-to-no trauma and the patient is healthy with few underlying conditions, very few side

effects have been reported for larger angle of insertion other than postoperative vertigo and nausea [126].

1.5 Finite element method

The finite element (FE) method is a numerical method which allows discretization and analysis of partial differential equations which may other be impossible to solve analytically. Applicable problems include ones with complex geometry, nonlinear material properties, and complex loads; ultimately, most any mechanical analysis problem can be solved using the FE method. When examining geometries derived from medical scans, the finite element method, or an analogous method like the finite volume method, is the ideal approach. The FE method is commonly employed in structural analysis, heat transfer, fluid flow, acoustics, and biomechanics.

1.5.1 Advantages over In Vivo testing

The use of laboratory animals is a necessary part of medical research, as it enables scientists to explore new treatments before progressing to human trials. However, animal testing is a complex issue that raises many ethical and logistical concerns, particularly regarding the welfare and cost of laboratory animals. Animal testing must be carried out in accordance with strict ethical guidelines to ensure that any suffering is minimized [39]. In medical research it is often necessary to purchase many expensive research-grade animals, making their use particularly expensive, especially when considering long-term management of an animal facility [16]. Furthermore, the quality of laboratory animals can be compromised by unethical practices, making studies less productive and reproducible.

Chinchillas are very often used in auditory research as a model for human hearing prior to progression to testing with non-human primates [122]. At the

time of writing there are very few laboratory grade chinchilla suppliers which are available to US researchers as many have been shut down by the USDA. One example is the Moulton Chinchilla Ranch, once the primary supplier of research grade chinchillas in the United States, which made a number of known violations of the Animal Welfare Act in the eight years prior to the revocation of their license [128]. Demand for chinchillas remains high; chinchillas are a valuable animal model for human hearing and balance function. There is a wealth of literature in the field which uses them as their subject, providing a foundation for further works to build on. The majority of research grade chinchillas must now be bred in house, prohibitive for many institutions due to logistics and cost.

Rhesus monkeys are the most commonly used nonhuman primates in biomedical research [55], due to their similar biology to humans [23]. However, unlike rodents, they are highly social animals with unique needs [4]. Rhesus monkeys are intelligent and capable of experiencing pain and suffering similar to humans. As a result, they are more heavily regulated and receive better treatment than small rodents. Partly due to these reasons, they are remain prohibitively expensive and too challenging to maintain for many labs.

Finite element modeling is a solution to both the monetary and ethical problems involved in animal research [36, 76]. FE modeling is cost-effective, ethical, reproducible, and safe. Models can be precisely manipulated at will in a relatively short time frame to account for a variety of different variables and conditions, some of which may not be foreseen prior to beginning modeling. Simulations can be run as many times as researchers desire with little-to-no variation in the model's geometry between iterations, something impossible when using multiple animals in a study [3]. In animal testing this kind of iterative process is also be quite expensive,

involving the purchase of many animals. The FE method can be applied without any harm to the animal subjects as medical imaging of delicate structures can be obtained non-invasively. Imaging can be shared among institutions, further reducing the number of animals needed for FE modeling. While not a replacement for animal testing, it is clear that in early stages of research the FE method should be explored prior to In Vivo testing on animal or human subjects.

1.5.2 Mathematical Basis

This work focuses on acoustic harmonic finite element analysis though the software ANSYS Mechanical [5]. Specifically, the ACT acoustics extension described in Acoustic Analysis Using MATLAB® and ANSYS® [60]. This section, and the study as a whole, relies heavily on the information contained in this book. Acoustic harmonic analysis is a method for quantifying the acoustic or vibration response of a system as a result of sinusoidally varying driving forces. In the application used here, the driving force is the vibration of the oval window membrane of the cochlea. The desired result is the vibration response of the basilar membrane. Frequency is held constant for each separate simulation. Two approaches are common when applying the FEM to acoustic harmonic problems: modal superposition and full solution.

Modal superposition is a method which is usually applied to simpler geometries where the body has vibration modes ψ_n. Modes are multiplied by a modal participation factor, P_n, and summed to find the total response of the structure, $\sum P_n \psi_n$. With a large enough number of modes any acoustic response can be represented. Though modal superposition can reduce the computing power necessary to run complex simulation, it is not currently supported by the ANSYS® acoustic

harmonic response module. Therefore a full solution must be calculated.

A full solution for nodal displacements $\{\boldsymbol{u}\}$ in the system requires the global mass $[\boldsymbol{M}]$, damping $[\boldsymbol{C}]$, and stiffness $[\boldsymbol{K}]$ matrices of the system in addition to the loading vector $[\boldsymbol{f}]$. Global matrices are formed from element matrices which describe each discrete elements behaviour given their respective prescribed boundary conditions, loading vectors, and material properties [40, 60].

The stiffness matrix is a symmetrical matrix which gives the relation between an elements internal forces and the displacement of its nodes. It is primarily derived from the elasticity and dimensions of the element. The damping matrix describes the decrease in the amplitude of oscillations as energy is drained from the system and is primarily informed by the β-damping coefficient in this work. The mass matrix describes the constant mass of each element throughout the simulation dependant on the elements volume and density. They are assembled together into the dynamic equation of motion describing an acoustic system, seen in Equation 1 [60, 102].

$$[\boldsymbol{M}]\{\ddot{\boldsymbol{u}}\} + [\boldsymbol{C}]\{\dot{\boldsymbol{u}}\} + [\boldsymbol{K}]\{\boldsymbol{u}\} = \{\boldsymbol{f}\} \tag{1}$$

$\{\ddot{\boldsymbol{u}}\}$ is equal to $-\omega^2\{\boldsymbol{u}\}$ and $\{\dot{\boldsymbol{u}}\}$ is equal to $j\omega\{\boldsymbol{u}\}$. This yields Equation 2.

$$-\omega^2[\boldsymbol{M}]\{\boldsymbol{u}\} + j\omega[\boldsymbol{C}]\{\boldsymbol{u}\} + [\boldsymbol{K}]\{\boldsymbol{u}\} = \{\boldsymbol{f}\} \tag{2}$$

The solution is obtained by separating out $\{\boldsymbol{u}\}$, seen in Equation 3, and then inverting the combined matrix while multiplying by the load vector to calculate nodal displacements, seen in Equation 4. This procedure is sourced directly from Acoustic Analyses Using MATLAB® and ANSYS® by Howard and Cazzolato [60].

$$(-\omega^2[\boldsymbol{M}] + j\omega[\boldsymbol{C}] + [\boldsymbol{K}])\{\boldsymbol{u}\} = \{\boldsymbol{f}\} \tag{3}$$

$$\{\boldsymbol{u}\} = (-\omega^2[\boldsymbol{M}] + j\omega[\boldsymbol{C}] + [\boldsymbol{K}])^{-1}\{\boldsymbol{f}\} \tag{4}$$

1.5.3 Prior Applications in Cochlear Mechanics

Over the past decade, substantial research progress has been made to advance inner ear computational modeling. Specifically, FE modeling has allowed the intricacies of the inner ear's mechanics to be reduced to simpler phenomena that can be verified with clinical results. In the case of inner ear mechanics it is almost always impossible to evaluate problems analytically due to the complex geometry of the cochlea and vestibular system. For this reason, numerous FE models of the inner ear have been made with a variety of different applications. Some of these applications have been noise-induced hearing loss, age-related hearing loss, broader cochlear mechanics in healthy cochleas, and cochlear implantation.

One model has been described which analyzed the association between noise exposure with hearing loss. This model had two and a half turns of the cochlea with three separated chambers for each of the scalae of the cochlea. It also include the ear canal and the middle ear, although no vestibular system was present. It provided valuable data on blast-induced auditory trauma and was an improvement on a prior two-chambered model of the cochlea by simulating some of the finer complexities of cochlear mechanics [17]. Another computational model described the association between age and hearing loss using a model of the human ear canal, middle ear, and simplified inner ear. The only parameter that was varied was the elasticity of the tympanic membrane; however, in reality, other parameters do change as one ages. This model demonstrated a significant difference in the

displacement of the stapes and was valuable in that it could inform development of artificial auditory ossicles [138]. One two-chambered model of the cochlea explored bone conduction in a spiral shaped model of the cochlea. Instead of the typical oscillation of the OWM as the input, vibration of the entire temporal bone which bounded the model was also applied. It was found that hearing sensation can actually be cancelled if both air conduction through the OWM and bone conduction are implemented simultaneously [14]. This model was a repurposed version of a previously described model based on imaging of the human inner ear which examined the simple propagation of acoustic waves through the ear. This model demonstrated the utility of inner ear FE models as easily modifiable and flexible tools for analysis [13].

Several models have focused specifically on the mechanics of the inner ear after CI surgery. One model used a spiral three-chambered cochlea with a variable circular cross section, also including a bulbous structure representing the vestibular system, though internal vestibular structures were omitted [140]. This model also included an accurate middle ear cavity and ear canal. This model found a large reduction of BM displacement along the length of the cochlea occupied by a simplified CI electrode, also with a variable circular cross section. BM displacement prior to CI surgery was validated and found to be quite accurate. This model provided a good first step towards further FE analysis of residual hearing after CI surgery, though did not necessarily agree with the results of other models where residual hearing was found to be less effected by the simple presence of a CI electrode and more effected by the trauma caused during insertion [6, 103]. Other models of cochlear mechanics after CI surgery were more focused on the trauma of insertion of the electrode. One such model found that material, geometric design, insertion

speed, and friction coefficients were the greatest factors influencing residual hearing preservation [6]. A previously developed finite element model focused on residual hearing found that cochlear implants most dramatically affect residual hearing at extreme frequencies of human hearing [78]. These factors are important considerations in clinical practice when choosing between pre-curved and straight electrode arrays; the study found that straight electrodes with low elasticity were the ideal choice to minimize effect of CI surgery on residual hearing, though other similar models have found that pre-curved electrodes result in better clinical outcomes [6].

1.6 Research Objectives

Hearing loss is clearly an issue which effects a large number of people. All options to combat this issue need to be carefully explored and every ramification thoroughly investigated. The focus of this study is to determine the effect of CI surgery on the residual mechanical hearing function of the inner ear. This is a neglected issue despite the fact that residual hearing function can have a large effect on patient outcomes. Previous models have not examined the effect of varying cochlear electrode insertion angles between patients. They also have not explored the residual hearing of non-human primates after CIS, and very few have accounted for vestibulo-cochlear interaction by including both the cochlea and vestibular system. These unexplored results could provide important metrics for later stages of research and for clinical use. Therefore, comprehensive finite element models capable of simulating hearing function with a variety of insertion angles and in novel species is an essential step in the improvement of cochlear implant design and surgery.

This work will explore the ramifications of CI surgery in two animal models, the

chinchilla and the rhesus macaque. These animals both possess inner ear anatomy and physiology which are well known to mirror that of the human inner ear. The powerful FE method is leveraged to allow for rapid and thorough analysis. The effect of insertion angle is explored in the chinchilla FE model. Previous models did not examine the effect of varying cochlear electrode insertion angles between patients. These unexplored results could provide important metrics for clinical use. Therefore, a comprehensive finite element model capable of simulating hearing function with a variety of insertion angles is an essential step in the improvement of cochlear implant design and surgery. The effect of CI surgery is examined more holistically in the rhesus macaque model with a set insertion angle, a finer mesh, and more accurate geometry. Both models are intended to reduce the necessity of large-scale animal testing in the industry by providing preliminary results without the use of animals. Both models can be altered quickly and efficiently to examine the effect of different disorders which may arise as a result of CI surgery. Both models represent a step forward in the field of inner ear FE modeling, with detailed inner ear anatomy of the cochlea and vestibular system. With these models, CI design and surgical procedures can be further improved to maximize patient outcomes, in hearing quality and in quality of life.

2 Methods and Procedures

The general method used to create the two finite element models presented in this work are quite similar. The methods presented here are an improvement on previous work in the Hearing and Balance Laboratory at the University of Oklahoma. Figure 4 displays the previous models as well as the chinchilla and rhesus macaque models focused on here. Figure 41-4 show prior models created in

our lab, focusing solely on the lymphatic fluid of the inner ear in various animal subjects. Though useful, these models cannot properly investigate the reaction of the membranes of the inner ear to sound, and therefore are not sufficient to achieve the aims of this study. Figures 4-5 & 4-6 showcase the models presented in this work. The membranes of the cochlea and vestibular system are visible, allowing for a more thorough analysis of inner ear mechanics.

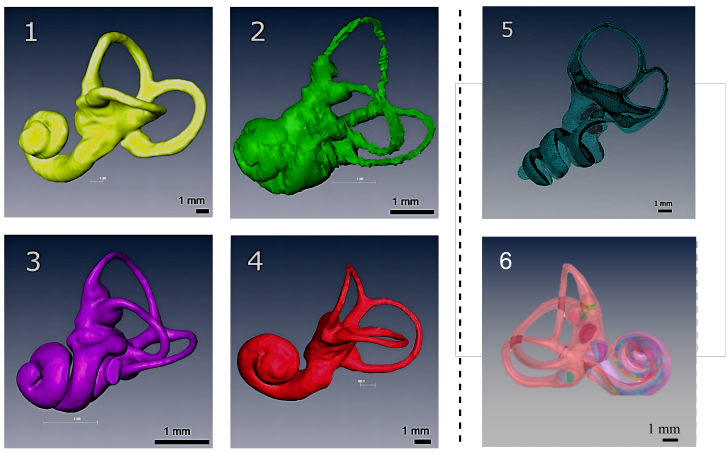

Figure 4: A history of inner ear FE models created in our lab, with the addition of the two models discussed in this work. The study protocol for all models was approved by the Institutional Animal Care and Use Committee of the University of Oklahoma following the guidelines of the National Institutes of Health and the US Department of Agriculture.

Special care was taken to use free, open-source software wherever possible to make this procedure modifiable and reproducible by other institutions and in future work in our lab. The procedures and methods outlined here can be expanded upon and applied to most any organ or tissue in the body for mechanical analysis.

2.1 Data Source & Segmentation

Magnetic resonance imaging (MRI) scans are the most valuable data source in creating mechanical FE models of biological structures. MRI's produce cross-sectional images of the body's soft tissues, vital to the recreation of membranes and small bones. MRI revolves around the manipulation of hydrogen nuclei, usually associated with water in the bodies tissues, using strong magnetic fields and radio waves. A simple diagram of MRI signal intensity dependant on fat and water content is shown in Figure 5.

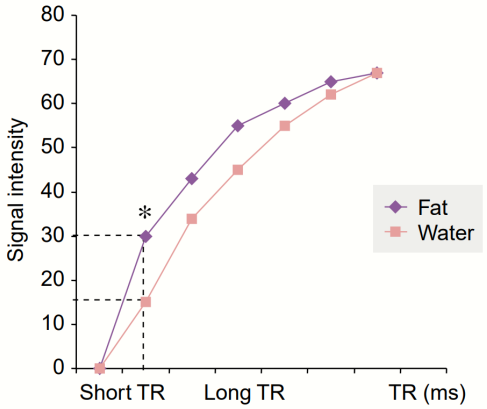

Figure 5: μMRI signal intensity depending on soft-tissue fat and water content. Adapted from The year(s) of the contrast agent - micro-MRI in the new millennium, by Pautler and Fraser with permission from the corresponding author and Elsevier on behalf of Current Opinion in Immunology [95].

When MRI was invented in an experimental setting in 1946 it represented a massive leap forward in technology, earning both inventors, Bloch and Purcell, a Nobel Prize for Physics in 1952 [9, 98]. Clinical MRI's were produced in 1980 by Nottingham and Aberdeen [56, 116] Since then, the technology has become widely accessible to clinicians. Now it is a staple of research and diagnoses of many

diseases.

μMRI scans present finer resolution images than a typical MRI scan, especially helpful for organs where important structures are close together and difficult to distinguish from one another. Spatial resolution can reach to the micron level. Examples of μMRI use include imaging of neurovasculature, clinical diagnoses of small vessel diseases, gene expression, imaging of individual cells, and isolation of complex geometries [15, 64, 90, 95]. μMRI scans were used in the creation of both models presented here.

CT scans are also useful as a tool in segmentation of medical scans. CT scans make use of X-rays, are less expensive than MRI scans, and are most useful in diagnoses of tumors, traumatic injuries to organs, and bone fractures. CT scans do expose patients to radiation, around 20 mSv whereas a significantly increased cancer risk is usually associated with does above 100 mSv [82]. The likelihood of developing cancer as a result of CT scans is therefore low, especially with modern developments. It is still important to be wary of excessive CT scanning of a patient, especially in pediatric patients where radiation can be more dangerous.

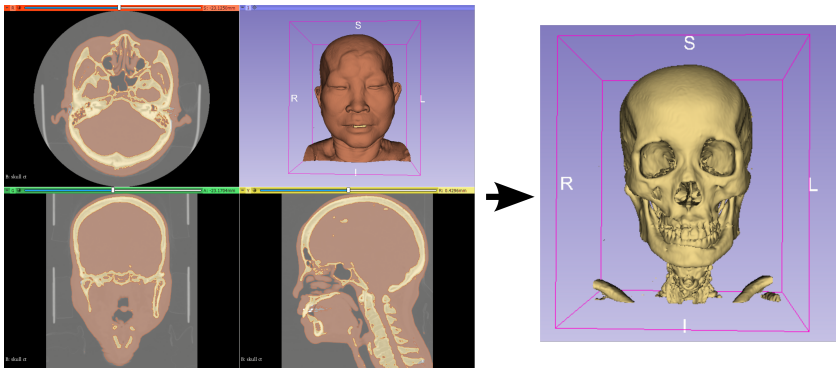

Figure 6: Example of a CT scan segmented using the software 3D Slicer. Medical imaging was used with the consent of the patient who preferred to remain anonymous.

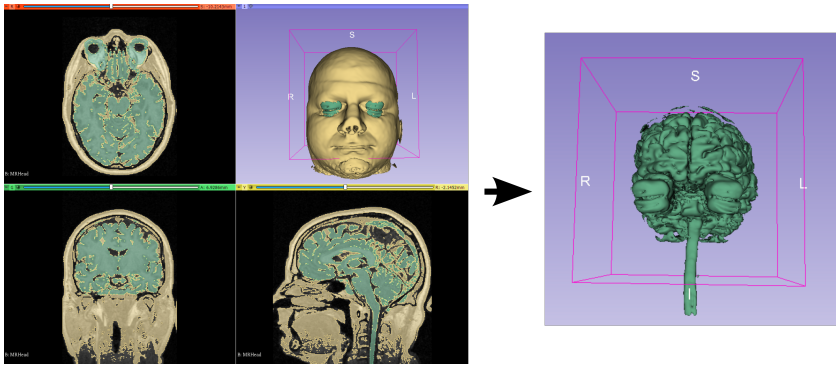

Figure 7: Example of an MRI scan segmented using the software 3D Slicer. Medical imaging was used with the consent of the patient who preferred to remain anonymous.

3DSlicer was used for segmentation of medical scans in order to generate point clouds from which surfaces could be extracted. 3DSlicer is a free open-source software which is easily accessible and has become a staple of quantitative analysis in clinical research [38]. 3DSlicer allows the creation of accurate 3D models of organic structures. It has seen use in teaching, where models can help students to visualize the anatomy and physiology of the body, finite element analysis, as it is applied here, and numerous other applications.

Segmentation can be done several ways in 3DSlicer. A global filter can be applied using the threshold tool to isolate tissues of a certain density. This can be especially helpful in segmenting bones and other larger structures where fine precision is not necessarily as important. An example of an ideal application for this tool is seen in Figure 6, where the skull is isolated from a CT of the skull. Finer tools are necessary for the inner ear and μMRI scans in general. The paint tool allows the user to either segment in 2D or 3D with a variable brush size where densities in the target tissues may vary. The paint tool is also useful where

simplifications of structures may be necessary, as was the case in separating the BM from the organ of corti. Level tracing works similar to the threshold tool but allows singular structures of a certain density to be selected. This can be applied in the separation of the membranous labyrinth of the vestibular system from surrounding structures without also including the membranes of the cochlea. The process of segmentation can be tedious and may take many man-hours as it did in the creation of the chinchilla and rhesus models of this paper. However, the fine control 3DSlicer offers allows the creation of very accurate models tailored to the users specific application.

For the models featured here, the lymphatic fluid was isolated from nervous and osseous tissue. As the lymphatic fluid fills the entire cochlea, key features could be identified such as the location of the OWM and RWM, path of the BM, path of the RM, and general shape of the utricle and semicircular canals of the vestibular system. These fine membranes perpendicular to the surface present as small gaps in the lymphatic fluid while larger depressions correspond to membranes parallel to the surface, like the OWM and RWM. These structures dimensions were further informed by extensive literature research.

2.2 Post-Processing

Though the point cloud generated by 3DSlicer can be very accurate, there are often imperfections in surfaces which must be corrected prior to further processing of the model. MeshMixer was used to correct these imperfections. MeshMixer features many smoothing tools and the ability to close gaps in the model. The final result of this post-processing process is a 2D surface that can be further altered during the meshing process.

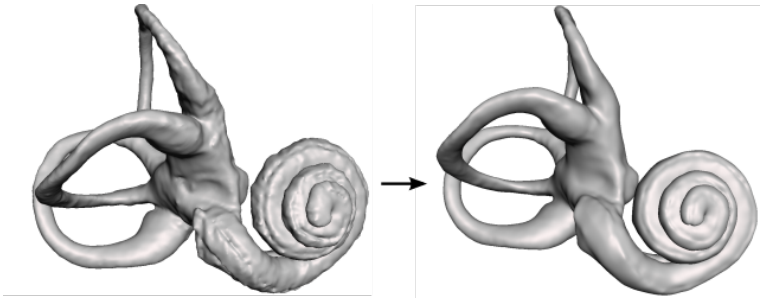

Figure 8: Example of the use of MeshMixer to smooth the rhesus inner ear model discussed in this work

After the general geometries of all structures are isolated and exported as .stl files, they must be reverse-engineered to form parametric surfaces. This procedure allows for automatic meshing at user-defined element sizes in 2D. This process was accomplished in Ansys SpaceClaim using the 'skin surface' tool. The outer surface of each structure is parametrized by creating 'patches', small sections of the overall surface which must be knitted together to form the final, continuous surface spanning the entirety of the structure of interest. The boundaries of each patch are carried over into the meshing process, defining a section which is designated its own element size. An example is shown in Figure 8.

2.3 Meshing

The most intensive process of the creation of inner ear models is meshing. As discussed previously, this process allows discretization of the partial differential equations solved during simulation of the model and must be done with care. Free meshing software can be found but lack the precision needed for this application. Therefore, HyperMesh was selected as the software used for this process. HyperMesh is a software created by Altair and is touted as a 'high-performance finite

element model pre-processor to prepare even the largest models, starting from import of CAD geometry to exporting an analysis run for various disciplines.' [61] This process will be more thoroughly explored for each model in their respective sections.

First, the outer surface of all structures must be meshed in 2D. A suitable mesh element size must be selected for the application. In modeling of inner ear mechanics this mesh must be fine to account for irregular geometry and must be especially fine for the most important structures, in this case the BM, RM, and OWM.

Next, a 3D mesh must be generated. For key structures this must be done with high accuracy, where thicknesses may vary and depend on values presented in literature. One example is the BM, which has a variable width and thickness along its length. All membranes in the models presented here fall into this category. 3D structures must also be connected, ensuring that nodes are shared between each with minimal change to the existing 2D mesh. The final 3D structures to be generated were the endolymph and perilymph, guided by the outer face of the model, representing bone, and the faces of the inner membranes. The tissues and the electrode array of the model utilized the Ansys SOLID185 element type, while the fluids were modeled using the Ansys FLUID30 element type. All elements were tetrahedral. Both SOLID185 and FLUID30 tetrahedral elements have 8 nodes, each with 4 degrees of freedom, translations in the nodal x, y and z directions, and pressure. Translation degrees of freedom are applicable only at nodes on the interface between fluid and solid element types. Both SOLID185 and FLUID40 element types have been previously used with success in our lab [44, 74].

Applying mesh size convergence analysis to future iterations of the model may

reduce the computing power and time necessary for simulation [130]. The chinchilla model was able to run a full simulation of all selected frequencies in approximately 15 minutes with the processing power available in our lab. However, due to the very fine mesh size used in the rhesus model, it took approximately 30 to 35 minutes to run a complete simulation. We believe that a courser mesh size for both models could achieve similar results. To achieve this, the parametric surfaces of the model would need to define thicknesses of membranes and the attachment points between all structures so that the model could be easily re-meshed. This is not possible with the current method used to generate these models in HyperMesh. Higher order elements, such as Ansys SOLID186 and FLUID220, were also not feasible to use in this study given the limitations of HyperMesh. We hope to present an improved method in the future which has the capability for mesh size convergence analysis and the use of higher order element types.

2.4 Material Properties

Material properties for both models were obtained almost entirely from literature. The most important material properties for acoustic harmonic analysis of these models are elasticity and the β damping coefficient. The β damping coefficient was the only damping considered, causing most complex displacements and phase shifts in the model [12]. The β damping coefficient is also known as the constant stiffness matrix multiplier [22, 111]. It is commonly implemented in FE models of the cochlea, however it is very difficult to quantify before beginning analysis in large systems such as the models described in this work. This makes it especially prudent to be extracted from prior successful models to guarantee accurate results [24]. Elasticity is much easier to determine for most structures from literature, though

still without high accuracy as the membranes of the inner ear are notoriously difficult to conduct material testing on. In this model, as in many others, all structures were assumed to be isotropic. The sources of these material properties and the details of their assignments are discussed in the respective sections for each model.

2.4.1 Phenomenological Approach to Material Properties

A phenomenological approach was used for the material properties of the RM and BM in the chinchilla model and the BM and membranous labyrinth in the rhesus model. The phenomenological approach attempts to match the overall behaviour of a system with empirical data, without necessarily relying on first-principle physics. This approach is useful with convoluted systems, or in cases where there are many complex interactions between components [83]. In the context of this work, mechanical properties were altered each run to produce results which match empirical data for the tuning effect of the cochlea obtained In Vivo, rather than using material properties directly measured in subjects. This is especially applicable in inner ear FEA because the material properties of many structures are difficult to find and therefore poorly defined in literature. Ideally, all material properties would be known and applied directly for more detailed results, and this is a target for future models in our lab. Material properties were altered so as to match the results described in the Greenwood frequency-position function.

The Greenwood frequency-position function, $F = A(10^{ax} - k)$, gives the resonant frequency at a given point along the BM [53]. F is the resonant frequency in Hz, A is a constant that varies by species' BM length, a and k are set constants, and x is the ratio of the chosen point's distance from the cochlear apex over the

total BM length. The mechanical properties of the model's basilar membrane (the elastic modulus and β-damping coefficient) were adjusted until the location of maximum BM displacement mirrored the frequency-position function's estimations. At this point, the model was said to be accurately tuned and prepared for simulation with the addition of the CI electrode.

2.5 Boundary Conditions

Boundary conditions were assigned following the example of previous models developed in the Hearing and Balance lab at the University of Oklahoma using the conditions available from the ACT acoustics extension [44,60,75]. The lymphatic fluids endolymph and perilymph, the primary media through which acoustic waves travel in the inner ear, were assigned as non-compressible fluid acoustic bodies. Elements of acoustic bodies have pressure degrees of freedom, but do not have displacement degrees of freedom except at interfaces with solid bodies, where fluid-sold interfaces are assigned. The fluid elements at these interfaces have both pressure and displacement degrees of freedom. All surfaces in contact with lymphatic fluid were designated as fluid-solid interfaces. The elements of the solid bodies, in these models the membranes and bones of the inner ear, have only displacement degrees of freedom. Fluid-solid interfaces are vital because they provide bi-directional coupling between vibrations of solid structures and pressure responses to traveling waves in the fluid acoustic bodies.

The most important boundary condition in the models described in this work was displacement of the oval window membrane. The displacement of the OWM corresponds to the output of the middle ear transfer function and is the input of all energy of the system. The middle ear transfer function describes the relationship

between the vibration of the tympanic membrane and the OWM, primarily determined by the structure of the middle ear. These displacements were pulled from studies in literature. A local coordinate system was created at the OWM of both membranes to ensure all displacement was in the normal direction of the surface of the OWM. The outer surfaces of both models were assigned as elastic supports, with stiffnesses determined by the material properties of the bony labyrinth which encases the inner ear. These supports were necessary constraints to obtain a closed solution.

3 Chinchilla Model

This study focuses on the effect of cochlear electrode insertion depth on the residual mechanical function of the cochlea in a chinchilla FE model. The unimplanted model is demonstrated here first and compared to expected response curves to demonstrate its initial validity. Analysis then focuses on the effects of cochlear implantation on residual hearing using the implanted model, with the insertion angle of the electrode varying from 180° to 900° in increments of 180°. The primary result of this study is frequency dependant locations of maximum displacement in the BM, a good measure of the tuning effect of the cochlea.

3.1 Chinchilla as an Animal Model

Chinchillas are commonly used as an analog for human hearing function due to their similar hearing range, inner ear structure, docile behaviour, and high genetic heterogeneity. [105, 122, 127]. The chinchilla hearing range of ≈30 Hz to 33 kHz is only slightly higher than the human hearing range of about 20 Hz to 20 kHz. Other commonly used rodents, like mice and gerbils, can have hearing ranges extending

past 80 kHz [123]. Therefore, chinchillas are a good model for the frequencies of sound relevant to human speech. A comparison between human and chinchilla audiograms is seen in Figure 9.

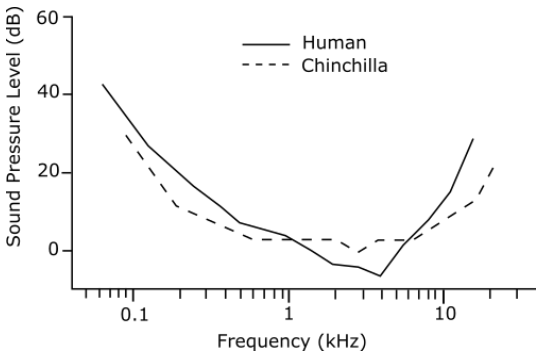

Figure 9: Comparison of human and chinchilla audiograms. [122]

Chinchilla cochlear anatomy is similar to humans in that they have three cochlear turns, whereas humans have 2 and three quarters turns. They also have a similar variation in length of the BM, around 30% [10]. This is in part due to the high genetic heterogeneity of chinchillas, as they are less inbred than other rodents that are typically used in animal studies. This makes chinchilla models a better representation of the variations seen between human inner ears. However, the average length of the human cochlea is about 31.5 mm whereas the chinchilla cochlear is only about 18 mm long.

Chinchillas can live up to 20 years in captivity, making them advantageous over other rodent species for both short- and long-term studies in auditory research. Their long life-span allows better research into age-related sensorineural hearing loss than is possible in other rodents [11]. They are docile in nature and easy to train, especially important in tests where it is helpful for animals to pay attention to, and give predictable reaction to, stimuli. They can be trained to detect changes

in acoustic simuli. They react very well to changes in sound intensity.

Chinchillas are especially useful in FE analysis due to their large auditory bulla, which allows for very fine resolution of models if scanned with a µ-MRI or µ-CT machine [122]. The middle-ear, cochlea, and RWM are easily accessible, making empirical measurements of hearing function and material properties possible. These anatomical properties have propelled many studies to utilize chinchillas, providing a solid base of literature to inform FE models of the chinchilla inner ear.

3.2 Data source & Segmentation

Model geometry was generated through 3D reconstruction of a single, adult chinchilla inner ear. μCT scans were acquired at 12 µm voxel size and μMRI scans at 30 μm voxel size. Achieving this voxel size with adequate reduction of feedback for the µ-MRI required 26 hours of acquisition in an 11.7 Tesla magnet. Images were segmented in 3D Slicer into lymphatic fluid, bone, and nervous tissue. Sample segmented μMRI and μCT images are seen in Figures 11 and 10.

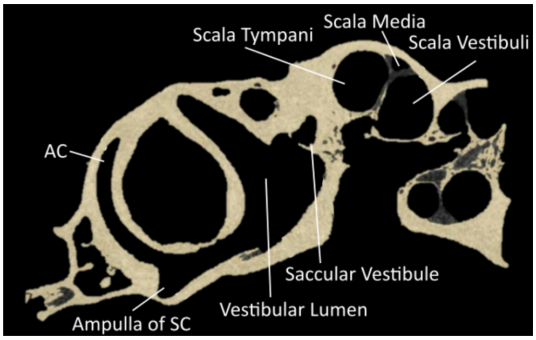

Figure 10: Segmented μCT scan in the sagittal plane of the chinchilla subject with key structures labeled. See Table 3 for symbol definitions.

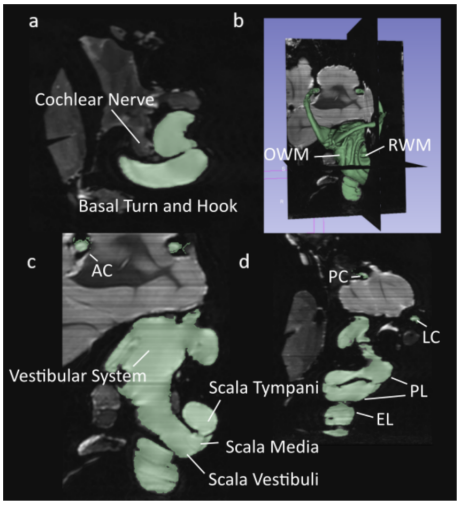

Figure 11: Segmented μMRI scans of the chinchilla subject with key structures labeled. See Table 3 for symbol definitions. The lymphatic fluid of the inner ear is shown in green. (a) Transverse plane (b) 3D view of the entire segmentation (c) Saggital plane (d) Coronal plane

Though μCT data was used as a secondary check on the boundaries of lymphatic fluid in the model, the geometry of this model was derived from segmented μMRI data and will be the focus of all further analysis in this section. The model derived from μMRI imaging is shown in Figure 12 after post-processing in MeshMixer.

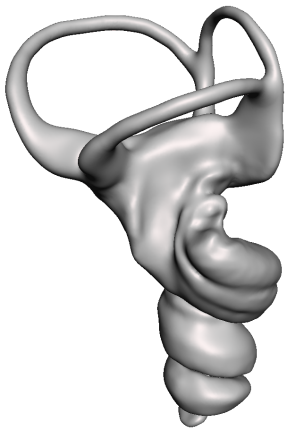

Figure 12: Lymphatic fluid of the chinchilla FE model after post-processing in MeshMixer. Curves corresponding to the attachment points of the RM and BM were preserved, as was the general shape and position of the OWM and RWM.

3.3 Geometry

The membranous labyrinth of the semicircular canals was modeled in MeshMixer by creating a copy of the bony labyrinth shrunk by a fraction to create two volumes, one enclosed within the other. The utricle's shape was modified to maintain proper connectivity with the semicircular canals and the ampullae. The utricle was scaled to accommodate a macula consistent with descriptions in literature [31, 79]. The saccule was modeled by cross-referencing measurements obtained for humans with data obtained on the saccular macula in the chinchilla [50, 115]. Cupula structures follow the diaphragmatic model and span the entire width and height of the ampullae. The diaphragmatic model is commonly used in the modeling of vestibular mechanics and yields results that closely mirror reality [67, 99, 136]. The reuniting duct was modeled according to measurements found in literature [100, 119, 137]. The coordinate system for all figures in this section are described in Figure 13. An annotated model of the completed vestibular system is illustrated in Figure 14.

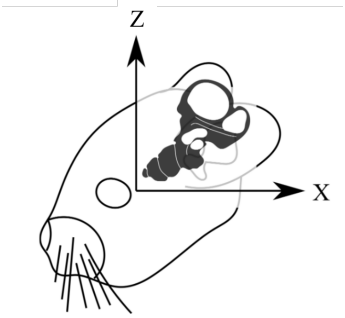

Figure 13: The coordinate system used in all imaging for the chinchilla FE model presented in this work. The x and z axes are held in the sagittal plane as if viewed from the subjects left side.

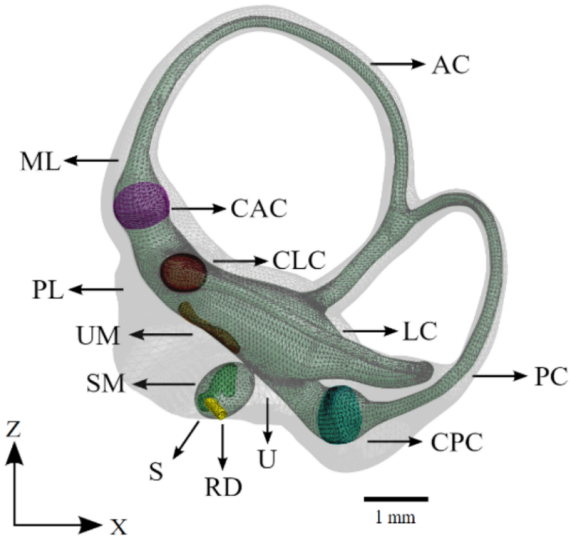

Figure 14: The vestibular system of the computational model. The saccule, utricle, and semicircular canals appear as a continuous volume of lymphatic fluid (green). The sensory organs of the vestibular system are also shown. See Table 3 for symbol definitions.

The cochlea was modeled primarily based on information obtained from µMRI imaging. Characteristic ridges on the surface of the bony labyrinth were used to

determine the attachment points of the RM and BM. The osseous spiral lamina was also clearly defined and marked the inner attachment of both the RM and BM. These curves were connected by planes, forming a wedge whose superior face represents the RM and whose inferior face represents the BM. This shape was compared with that seen in literature and was confirmed to have the correct structure [77] The completed model of the cochlea is displayed in Figure 15.

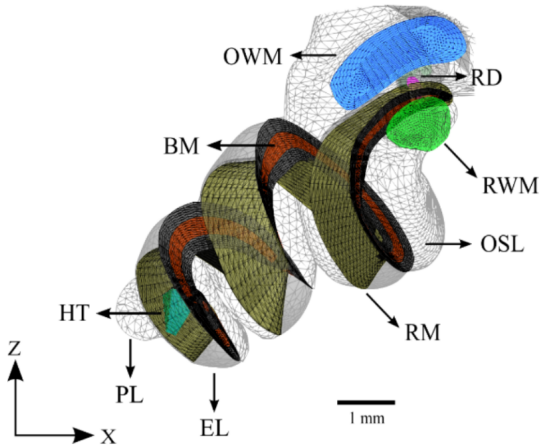

Figure 15: The cochlea of the computational model without cochlear implant. The design of the basilar membrane (red) is apparent as a ribbon with varying width and thickness, attached on both sides to bony supports (grey). The distal side of the basilar membrane is visible as the attachment point for the end of the reissner's membrane. See Table 3 for symbol definitions.

The cochlea was scaled until the BM was the average length in chinchillas of 18.3 mm along its midline [10]. The thickness of the BM was varied from 16.5 μm at the base to 5 μm at the tip according to the values given for the pars pectinata in Cochlear Anatomy and Central Auditory Pathways [108]. Dimensions of a MED-EL FLEXSOFT electrode array were scaled to create an analogous implant which

was placed in accordance with an ideal round window insertion in the scala tympani of the cochlea. The cochlear electrode extends almost the full length of the scala tympani with a maximum insertion angle of 900°. This implant was split into 180° sections to allow for analysis with varying angles of insertion. Cross sections at the proximal and terminal ends of the cochlear electrode are shown in Figure 16.

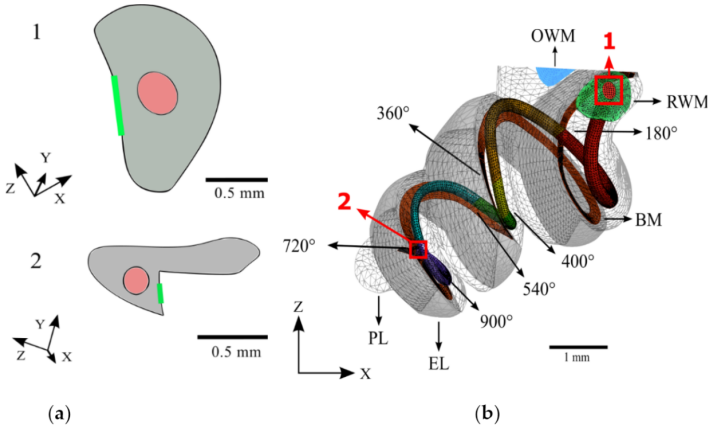

Figure 16: The full meshed model of the cochlea is presented with the length of the cochlear implant electrode inserted. (a) Cross sections of the base (1) and apex (2) ends of the cochlear implant electrode; (b) The path of the cochlear implant electrode through the scala tympani of the meshed model.

3.4 Meshing

The components relevant to the mechanical model were meshed, including: the oval window membrane, round window membrane, cupulae, maculae, basilar membrane, Reissner's membrane, utricle, saccule, semicircular canals, cochlea, and cochlear implant electrode array. All components were meshed in 2D and then given proper connectivity, assigned their respective thicknesses, and meshed with tetrahedral elements using HyperMesh. The mechanical model was meshed with

a total of 414,629 tetrahedral elements and 90,696 nodes using the software HyperMesh. Mesh size convergence analysis was not conducted due to the very fine average element size of about 0.2 mm, and the logistics of further modifying meshes of a model of this complexity. This mesh size is sufficient when considering the larger element sizes utilized by previous models [44, 75]. Tissues and the electrode array were modeled using the Ansys SOLID185 element type while fluids were modeled using the Ansys FLUID30 element type. As the BM was the most important component of this model, it was carefully meshed so as to maintain rectangular surfaces on all sides, maintaining uniformity across its length. It was split into 56 different segments, each with their own material properties to be changed dynamically during the tuning process. The meshed BM was composed of 5,343 tetrahedric elements and 2,019 nodes.

3.5 Material Properties

Due to the relative scarcity of published data on the material properties of chinchilla inner ear soft tissues, material properties measured in humans have been substituted as needed. All material properties are located in Table 1. The material properties of the endolymph and perilymph were assumed to be identical due to their similar composition. Mechanical properties of the RWM were gathered from Zhang et al. [139] and Gan et al. [43]. The RM and BM in this model have 0.4 as their Poisson's ratio. The RM and BM also have varied Young's moduli and damping factors along their lengths [87]. Exponential equations describing these quantities were selected to ensure the model's results most closely resembled the experimental results used as a baseline. These equations were determined through repeat simulation using different plausible functions dependent on position along

the cochlea.

The material properties of the cochlear implant electrode array were based on the Nucleus Straight electrode array as the material properties of the MED-EL models are not published. A Young's modulus of 0.4 MPa and density of 3400 kg/m3 were used as has been previously done by Lim et al. in their finite element model of residual hearing after cochlear implantation [78]. The damping factor of cochlear implant electrode arrays has not been published and was thus assumed to be that of the carrier material, silicone rubber [106].

Material properties of the endolymph and perilymph were assumed to be identical given their similar compositions. These properties were assigned as reported by Shen [113]. To our best knowledge, there is no published description of inner ear bone density for chinchillas. Therefore, the density of all osseous tissue was assumed to be 1200 kg/m3 as previously done by Gan in her human cochlea model with further support from Wang et al.'s conclusion that chinchilla bones have a lower density than human bones [44, 130]. The Young's modulus used for osseous tissue was 14.1 GPa as done in the human cochlea model reported by Wang et al. [129].

Structure	Parameter	Structure	Parameter
Basilar Membrane		**Membranous Labyrinth**	
Density (kg/m^3)	10^3	Density (kg/m^3)	10^3
Elastic Modulus (Pa)	$(7.1 \cdot 10^4)^{-.21x}$	Elastic Modulus (Pa)	$1.3 \cdot 10^4$
β Damping Coefficient	$(2.3 \cdot 10^{-8})^{.52x}$	β Damping Coefficient	.14
Reissner's Membrane		**Lymphatic Fluids**	
Density (kg/m^3)	10^3	Density (kg/m^3)	10^3
Elastic Modulus (Pa)	$10^4 \cdot x$	Elastic Modulus (Pa)	$2.6 \cdot 10^9$
β Damping Coefficient	$(6 \cdot 10^{-6})^{.158x}$	β Damping Coefficient	$1.5 \cdot 10^{-4}$
Cupulae		Viscosity (Pa·s)	10^{-3}
Density (kg/m^3)	10^3	Speed of Sound (m/s)	1498
Elastic Modulus (Pa)	2.8	**Oval Window Membrane**	
Maculae:		Density (kg/m^3)	10^3
Gel Layer		Elastic Modulus (Pa)	$3.5 \cdot 10^5$
Density (kg/m^3)	10^3	β Damping Coefficient	10^{-4}
Elastic Modulus (Pa)	10	**Round Window Membrane**	
Otoconial Layer		Density (kg/m^3)	$1.5 \cdot 10^3$
Density (kg/m^3)	$2.71 \cdot 10^3$	Elastic Modulus (Pa)	$3.5 \cdot 10^5$
Elastic Modulus (Pa)	500	β Damping Coefficient	$5 \cdot 10^{-4}$
Bone		**Cochlear Implant**	
Density (kg/m^3)	$1.2 \cdot 10^3$	Density (kg/m^3)	$3.4 \cdot 10^3$
Elastic Modulus (Pa)	$1.34 \cdot 10^{10}$	Elastic Modulus (Pa)	$4 \cdot 10^4$
β Damping Coefficient	0.45	β Damping Coefficient	$7.7 \cdot 10^{-2}$

Table 1: The material properties assigned to each component of the chinchilla FE model.

3.6 Boundary Conditions

The simulation domain was defined to encompass the fluid boundaries of the inner ear and the bony labyrinth, with the outer surface of the bony labyrinth being fixed to approximate its rigidity. Fluid-solid interfaces were defined for each solid face in contact with either endolymph or perilymph, and the acoustic properties of both fluids were defined to enable the propagation of acoustic waves. Harmonic acoustic simulation was then carried out using experimentally determined parameters for stapes footplate displacement in the human at 90 dB. A graph of stapes displacement dependant on frequency of sound is seen in Figure 17. Human stapes displacement was used as chinchilla stapes displacement dependant on frequency was unavailable from literature, as was done in the similar study by Gan et al. [44].

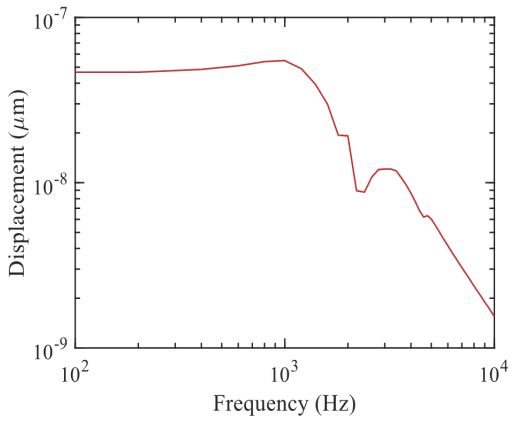

Figure 17: Displacement of the chinchilla model stapes at 90 dB dependant on frequency of sound at the tympanic membrane. [44]

The displacement of the BM perpendicular to its surface was then determined using specialized code in Ansys APDL and normalized by the displacement of the stapes footplate for further analysis. The boundary conditions for both the healthy and implanted models were identical for all components except the CI electrode.

In the healthy model, the CI electrode was designated as an acoustic body, assigned the element type FLUID30, and given the material properties of lymphatic fluid. For the implanted model the segments of the CI electrode pertinent to the given insertion angle had additional fluid-solid interfaces defined on their outer surfaces, they were unassigned as acoustic bodies, and their material properties were changed from lymphatic fluid to those defined in Table 1 for the CI electrode.

3.7 Results

3.7.1 Unimplanted Ear

Figure 18a shows the raw, unnormalized displacements of the basilar membrane at each tested frequency. Figure 18b shows the normalized magnitude of displacements along the cochlea. Excess noise was suppressed by applying a local filter across every 0.2 mm of the cochlea. This noise is to be expected at the overlaps of curves between two frequencies due to their differing wavelengths [124]. The majority of noise occurs towards the end of the cochlea as acoustic waves disperse, as seen in Figure 18a. This model may generate more noisy data due to the accurate triangular shape of the scala media. The magnitude of displacement of the basilar membrane decreases as frequencies become lower. This phenomenon can be explained by the heightened stiffness of the basilar membrane towards the base and has been observed in other studies [33, 71, 140].

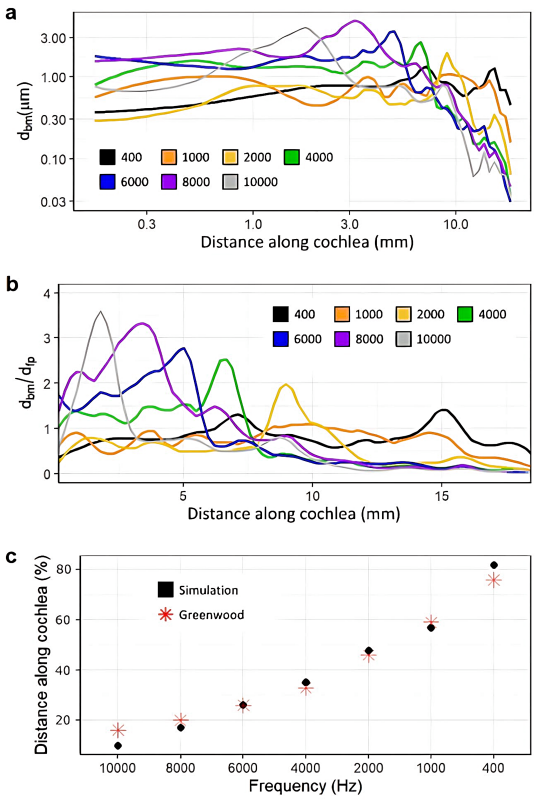

Figure 18: Displacement of the basilar membrane from base to apex of the cochlea before insertion of the CI. (400 Hz: black, 1000 Hz: orange, 2000 Hz: yellow, 4000 Hz: green, 6000 Hz: blue, 8000 Hz: purple, 10000 Hz: grey) Model input was experimentally determined frequency dependent displacement of the stapes at 90 dB [44]. 18a and 18b show unnormalized displacement of the BM and BM displacement normalized by that of the stapes footplate, respectively. 18c shows the location of maximum displacement for the model (black) at each frequency compared to an experimentally obtained benchmark [53].

The models' integrity was verified by comparison with the data set contained in the 1990 Greenwood study, a common source for data on the frequency and position-dependent displacement of the basilar membrane [53]. Figure 18c shows

the tuning effect of the model, gauged by the locations of maximum displacement. The plot exhibits a mostly linear, downward trend in the magnitude of displacement as frequency decreases and is very similar in locations of maximum displacement for all assessed frequencies compared with published results. This was important for analysis of the implanted model, as the tuning effect of the cochlea is vital to the proper perception of pitch [97, 124].

3.7.2 Implanted Ear

Results were collected for insertion angles between 180 and 900 degrees in increments of 180 degrees. Only results for a 180 degree and 900 degree insertion are shown in Figure 19 for the sake of brevity as all trials were very similar, other than the slight variation at 2000 Hz with the 900 degree insertion angle. Magnitudes of displacement varied only slightly with all insertion angles and locations of maximum displacement were almost exactly consistent with the results from the unimplanted model. They suggest that an ideal CI surgery with no trauma has the potential to have very little effect on residual mechanical hearing function. There were two major findings from these results: 1) The tuning effect of the cochlea is not significantly altered after the insertion of cochlear electrodes, representing an accurate perception of pitch. 2) The magnitudes of displacements in the BM are not significantly altered by the insertion of cochlear electrodes, representing an accurate perception of volume.

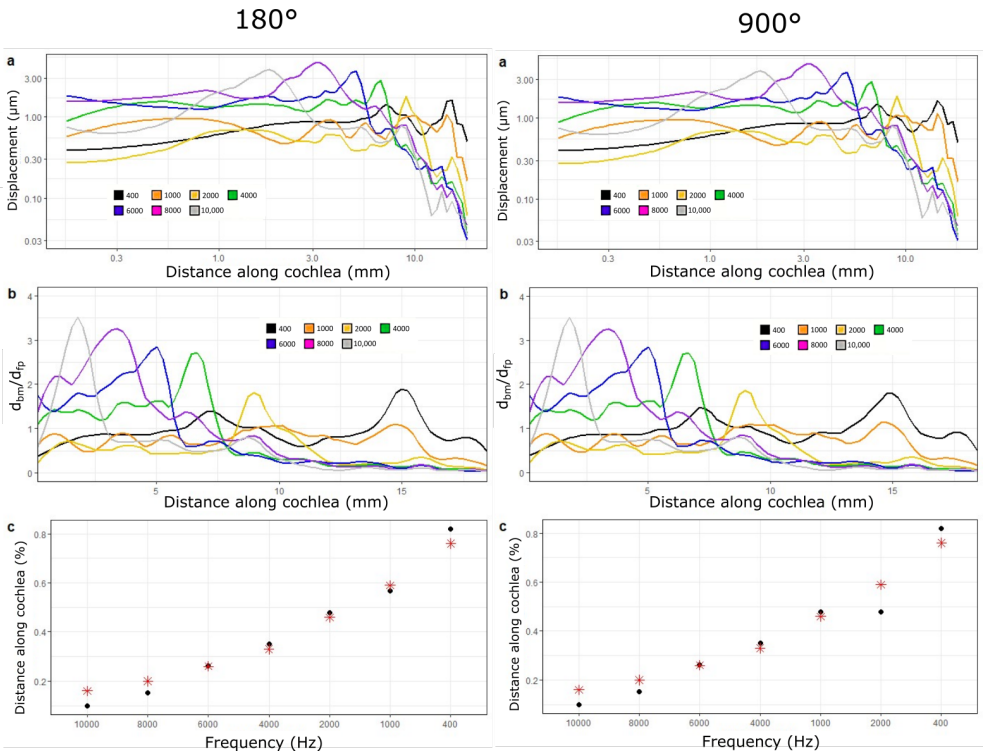

Figure 19: Displacement of the basilar membrane from base to apex of the cochlea before insertion of the CI. (400 Hz: black, 1000 Hz: orange, 2000 Hz: yellow, 4000 Hz: green, 6000 Hz: blue, 8000 Hz: purple, 10000 Hz: grey) Model input was experimentally determined frequency dependent displacement of the stapes at 90 dB [44]. 19a and 19b show unnormalized displacement of the BM and BM displacement normalized by that of the stapes footplate, respectively. 19c shows the location of maximum displacement for the model (black) at each frequency compared to an experimentally obtained benchmark [53].

4 Rhesus Model

This study focuses on a FE model of the rhesus macaque's inner ear, created to examine the effects of electrode placement on residual mechanical hearing function. This model is evaluated in a very similar manner to the previously discussed chin-

chilla model. The model is first analyzed in its unimplanted state and compared to data obtained In Vivo to demonstrate its validity. Then, the CI electrode is introduced and the differences between frequency dependant locations of maximum displacement in the BM are studied. Work on this model is ongoing. Initial results are shown here to demonstrate the promise it holds for future analysis.

4.1 Rhesus Macaque as an Animal Model

Non-human primates in general are accepted as the gold-standard of animal models for human audition, especially Old-World monkeys given how closely related they are related to humans. For this reason, non-human primates share much of our physiology and susceptibility to infectious diseases of the inner ear [21]. They can learn complex tasks quickly through positive reinforcement and perform these tasks accurately. They also share similar hearing ranges with humans. The hearing range of the rhesus monkey is approximately 40 Hz to 40 kHz, about an octave higher than the human hearing range of about 20 Hz to 20 kHz [93] . Rhesus monkeys have a similar audiogram shape to humans, though have a less sensitive range around 4 kHz which is exhibited in most studies of non-human primates [25]. Humans and rhesus monkeys have a singular range of high hearing sensitivity, from about 500 to 4000 Hz in humans, the primary frequencies of human speech, and from about 1000 to 16000 Hz in rhesus monkeys [58, 96] Audiograms for humans and rhesus monkeys can be seen in Figure 20, with the range of greatest sensitivity approaching a sound pressure level of 0 dB.

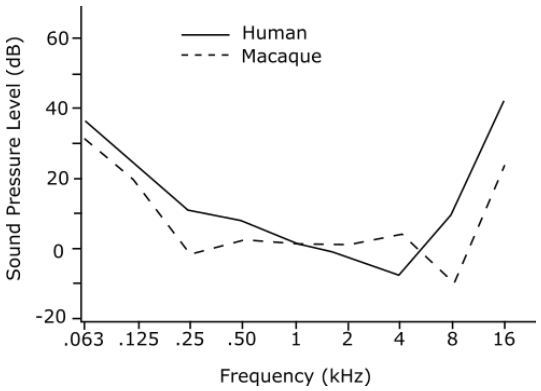

Figure 20: Comparison of rhesus and human audiograms. Adapted from Coleman [25].

The major structures of the cochlea are very similar across all non-human primates given our genetic similarity. However, specific volumes and dimensions vary, such as the length of the cochlea, fluid volumes, and size of ducts [28]. Specific dimensions of delicate structures are more difficult to study in comparison to rodents rodents given the strict regulation of rhesus monkey animal testing. This is one downside to their use as an animal model for FE modeling. However, their many similarities in general structure and the common use of rhesus monkeys as a model for human audition make them especially useful for FE modeling of later stages of animal testing. There is a large amount of literature which can be relied upon for expected results and desired inputs of such a model. Therefore, a FE model of the rhesus monkey inner ear is an important step in ethical and efficient development of cochlear implants.

4.2 Data Source & Segmentation

The geometry for the model was sourced from μMRI data sets of the rhesus macaque. As these scans had higher resoltion than those of the chinchilla model,

3D Slicer was used to directly segment regions of interest, including: the utricle, saccule, membranous labyrinth stria vascularis, osseous spiral lamina, and lymphatic fluids. Nervous tissue was also isolated for use in later studies.

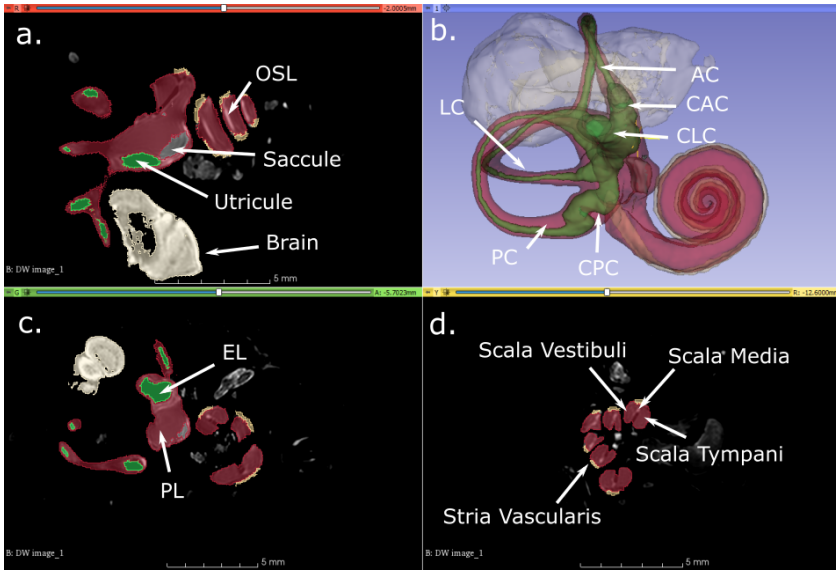

Figure 21: Segmented μMRI scan of the rhesus monkey inner ear with key structures labeled. The vestibule is shown in green, perilymph in red, saccule in grey, and stria vascularis in yellow. See Table 3 for symbol definitions.

The 3D geometry acquired from 3D Slicer was imported into MeshMixer, wherein the model was smoothed and repaired. Portions of the anterior semicircular canal were especially poorly defined due to lack of resolution in those areas of the medical imaging, but were repaired and made to match the dimensions of the lateral and posterior canals in MeshMixer.

Figure 22: The smoothed model of lymphatic fluid in the rhesus model.

4.3 Geometry

The macaque's lymphatic fluid volume is 31% of the human's, so the lymphatic fluid isolated from medical imaging was scaled to match this value [28]. The RM and BM attach to prominent ridges within the cochlea and to the edge of the osseous spiral lamina, all of which were visible within the µMRI data set. Flat planes were created between connection sites to simulate the membranes. The average midline length of the BM in rhesus macaques is 26.39 mm [19], which matches the measured value of 27 mm after scaling the model based on the ratio of rhesus to monkey lymphatic fluid volumes. The width of the BM was found to be 0.27 mm at the base of the cochlea and 0.46 at the apex. The RM thickness was set to a constant .012 mm across its length [114]. Unlike the previous model, the stria vascularis on the lateral wall of the cochlea was included to determine if its damping properties would have a significant effect on results. The stria vascularis was accurately isolated from the μMRI data set. The osseous spiral lamina was isolated directly from μMRI imaging and verified with literature [101]. Multiple sources were cross-referenced to model the helicotrema accurately as it was not

well defined in our imaging [81, 134]. The derived values for the length and width of the helicotrema are 0.20 mm and 0.15 mm, respectively.

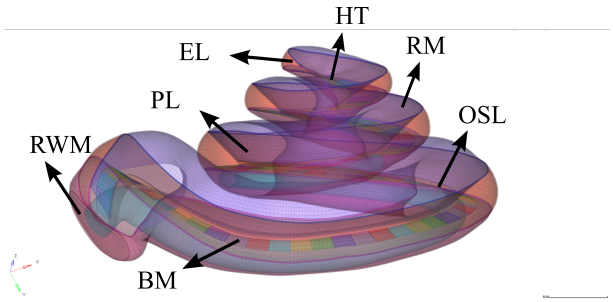

Figure 23: The meshed version of the rhesus model cochlea with annotations for all key structures. See Table 3 for symbol definitions.

The saccule's structure was unclear from imaging; its dimensions had to be extrapolated from what was visible in the data sets. However, measuring the volume and cross-referencing with literature seemed to indicate that the geometry was accurate [86]. The same was done for the reuniting duct [73], which connects the saccule to the cochlea. There is little literature on the utriculosaccular duct, which connects the saccule to the utricle, and so its diameter was assumed to match that of the reuniting duct. The RWM and OWM thicknesses were set to be 0.05 mm, per Goyocoolea's findings on the macaque's round window membrane [52]. The shape of the RWM and OWM were determined directly from μMRI imaging.

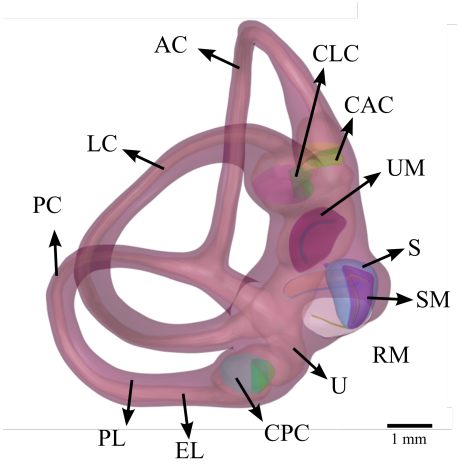

Figure 24: The meshed version of the rhesus model vestibular system with annotations for all key structures. See Table 3 for symbol definitions.

The maculae could not be isolated from our μMRI data. Using data from Igarashi's 1975 study on squirrel monkeys [63], the shape of the maculae were approximated. The maculae were scaled from the dimensions obtained for human subjects as a factor of the volume of the vestibule to approximate rhesus monkey anatomy [27, 62, 104]. The thickness of the maculae was set to 0.05 mm [8]. By measuring the size of the ampullae isolated from μMRI scans, and cross-referencing with the dimensions of the human ampullae and cupulae, accurately dimensioned cupulae were created [26]. The diaphragmatic model of the cupula was implemented in this study, as has been commonly done in other inner ear FE models [67, 99, 136].

4.4 Meshing

Geometry from MeshMixer was imported to SpaceClaim to create skins of each surface. Components included: the RM, BM, stria vascularis, cupulae, maculae, membranous labyrinth, osseous spiral lamina, and lymphatic fluid. Then, Hyper-

mesh was used to merge skins and mesh the model as previously described. The model ultimately consisted of 2,657,915 elements and 599,961 nodes, with an average element size of 0.075 mm. This mesh size is sufficient when considering the much larger element sizes utilized by previous models [44, 75]. The BM was split into 86 segments and carefully meshed with rectangular 2D elements and given thickness, creating a total of 4920 elements 8-noded brick elements and 10,846 nodes.

4.5 Material Properties

As literature on the mechanical properties of rhesus the inner ear is not complete, material properties of the human inner ear were substituted as needed. Though it was necessary to use human material properties in the chinchilla model, the rhesus inner ear is more closely related to the human inner ear making these values a better approximation for this use case [21]. A full list of all material properties used in this model is tabulated in Table 2. The BM material properties are most important to the behaviour of the FE model. In order to obtain optimal results, the elastic modulus and β damping factor of the BM are being tuned with the phenomenological method described previously. Like most of the tissues in this study, its density was set to 1.20E+03 $\frac{kg}{m^3}$ [139]. The membranous labyrinth density was also set to 1.20E+03 $\frac{kg}{m^3}$ [44] and its Poisson's ratio to .4 [67]. Similar to the BM, its elastic modulus and β damping coefficient are being experimentally determined. The endolymphatic and perilymphatic fluid are mechanically identical to water, and were approximated as such [89].

Structure	Parameter	Structure	Parameter
Basilar Membrane		**Membranous Labyrinth**	
Density (kg/m^3)	$1.2 \cdot 10^3$	Density (kg/m^3)	1.2^3
Elastic Modulus (Pa)	TBD	Elastic Modulus (Pa)	$1.3 \cdot 10^4$
β Damping Coefficient	TBD	β Damping Coefficient	0.14
Reissner's Membrane		**Lymphatic Fluids**	
Density (kg/m^3)	10^3	Density (kg/m^3)	10^3
Elastic Modulus (Pa)	13000	Elastic Modulus (Pa)	$2.6 \cdot 10^9$
β Damping Coefficient	0.005	β Damping Coefficient	$1.5 \cdot 10^{-4}$
Cupulae		Viscosity (Pa·s)	10^{-3}
Density (kg/m^3)	$1.2 \cdot 10^3$	Speed of Sound (m/s)	1498
Elastic Modulus (Pa)	5.4	**Oval Window Membrane**	
Maculae:		Density (kg/m^3)	$1.2 \cdot 10^3$
Gel Layer		Elastic Modulus (Pa)	$3.5 \cdot 10^5$
Density (kg/m^3)	$1.2 \cdot 10^3$	β Damping Coefficient	$5 \cdot 10^{-5}$
Elastic Modulus (Pa)	10	**Round Window Membrane**	
Otoconial Layer		Density (kg/m^3)	$1.2 \cdot 10^3$
Density (kg/m^3)	$2.71 \cdot 10^3$	Elastic Modulus (Pa)	$3.5 \cdot 10^5$
Elastic Modulus (Pa)	500	β Damping Coefficient	$5 \cdot 10^{-4}$
Bone		**Cochlear Implant**	
Density (kg/m^3)	$1.2 \cdot 10^3$	Density (kg/m^3)	$3.4 \cdot 10^3$
Elastic Modulus (Pa)	$1.34 \cdot 10^{10}$	Elastic Modulus (Pa)	$4 \cdot 10^4$
β Damping Coefficient	0.45	β Damping Coefficient	$5 \cdot 10^{-5}$
SAL			
Density (kg/m^3)	$1.2 \cdot 10^3$		
Elastic Modulus (Pa)	$2 \cdot 10^5$		
β Damping Coefficient	$5 \cdot 10^{-5}$		

Table 2: The material properties assigned to each component of the rhesus FE model.

4.6 Boundary Conditions

The simulation domain was defined to encompass the fluid boundaries of the inner ear and the bony labyrinth, with the outer surface of the bony labyrinth being

fixed to approximate its rigidity. Fluid-solid interfaces were defined for each solid face in contact with either endolymph or perilymph, and the acoustic properties of both fluids were defined to enable the propagation of acoustic waves. Harmonic acoustic simulation was then carried out using experimentally determined parameters for stapes footplate displacement in the human at 90 dB. A graph of stapes displacement dependant on frequency of sound is seen in Figure 17. Human stapes displacement was used as chinchilla stapes displacement dependant on frequency was unavailable from literature, as was done in the similar study by Gan et al. [44].

The displacement of the BM perpendicular to its surface was then determined using specialized code in Ansys APDL and normalized by the displacement of the stapes footplate for further analysis. The boundary conditions for both the healthy and implanted models were identical for all components except the CI electrode. In the healthy model, the CI electrode was designated as an acoustic body, assigned the element type FLUID30, and given the material properties of lymphatic fluid. For the implanted model the CI electrode had additional fluid-solid interfaces defined on its outer surface, was unassigned as acoustic bodies, and its material properties were changed from lymphatic fluid to those defined in Table 2 for the CI electrode.

4.7 Results

Ansys Mechanical is being used to perform harmonic-acoustic simulation on the model, as described previously. Current results from this model are not ideal as we have not properly tuned the material properties of the BM and RM with the phenomenological method described earlier. In this model the variables in the Greenwood frequency-position function, $F = A(10^{ax} - k)$, are A = 395, a =

2.1, and k = 1. A graph displaying the displacement of the BM normalized with stapes displacement in shown in Figure 25. Our results for the healthy model are improving, and we hope to have a close match between our results and the Greenwood function in the coming weeks. This is a long process as there are infinitely many possibilities for the BM and RM material properties, but currently we are testing a range of exponential functions for the BM elastic modulus and β damping coefficient using the general equation $E = a^{-b \cdot x}$ and $\beta = c^{d \cdot x}$, where x is the distance along the BM from base to apex. We are modulating a between 50 kPa and 100 kPa in increments of 10 kPa, b from -0.2 to -0.5 in increments of -0.05, c from $5 \cdot 10^{-5}$ to $5 \cdot 10^{-2}$ in increments of one order of magnitude, and d from 0.2 to 0.5 in increments of 0.05. This yields a total number of 540 different possible scenarios, though results from each trial inform the next. As each simulation takes approximately 30 minutes, this comes out to 11.25 days of constant time running simulations. That is without taking into account the variability of the RM material properties. We are currently developing a method which will allow us to automate this process, but when done manually we are only able to run about 10 simulations in a day. Once automated we hope to make use of the OSCER supercomputer to reduce runtime.

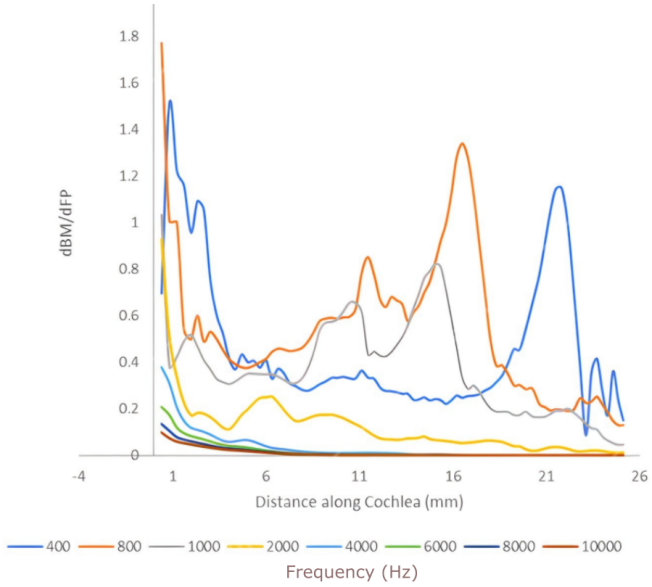

Figure 25: Normalized Displacement of the BM in the Rhesus Model. Each frequency is plotted in a different color according to the figure legend.

5 Discussion & Conclusion

5.1 Clinical Applications of the Models

Finite element analysis of the models in this study to date has two major implications in the mechanics of residual hearing after CI surgery: 1) CIS can have minimal effect on residual hearing. 2) The insertion angle of CIs, apart from their potential to physically damage the cochlea, has little effect on residual hearing. Literature on this topic is divided. Some studies have found CIS to have an effect on residual hearing, like Gan's model on the subject [44]. Others have found little to no long-term effect, especially in children. [133,140]. The general consensus is that without tip fold-over, displacement of the electrode, or some other fault, the effect of CI surgery on residual hearing is minimal [45,65]. Our results agree strongly with this conclusion. Insertion trauma is common, but it is not inevitable. While this model

does represent the best-case scenario of implantation, it does not detract from the applicability to electrode design. Furthermore, as surgery techniques continue to improve and additional technology is utilized, the rate of complications is expected to decrease and the importance of residual hearing will grow, thus these models will become more applicable in clinical settings [7].

It is desirable to create longer electrodes as they allow the patient to sense a wider range of frequencies more effectively [32, 33]. In the chinchilla model BM displacement was nearly unaffected in our chinchilla model regardless of CI electrode insertion angle. Results from this work support the theory that cochlear implants can have minimal effect on the mechanics of the BM, even when inserted into the apex of the cochlea. These results can inform CI electrode design; longer, more slender CI electrode designs should be prioritized to preserve residual hearing function. Results also suggest that the primary contributors to loss of residual hearing after CI surgery is cochlear trauma; CI insertion should be done as slowly and as carefully as possible. Iso-Mustajärvi's 2019 study provides another explanation for the very low effect of cochlear implantation on the chinchilla model [65]. He asserts that the primary contributor to the loss of residual hearing function after CI surgery, absent trauma, is the stiffening of the round window membrane. However, it may be that by tuning the model for optimal results in its healthy ear setting, some sensitivity to change in RWM stiffness was lost. A stiffer model of the RWM in the implanted state and a less stiff model of the BM may provide more answers. Further study will be required to confirm or deny this possibility, and we plan on studying this effect with the rhesus model described in this work.

5.2 Further Applications in Cochlear & Vestibular Mechanics

Compared to simplified two-chambered or straight cochlear models, the three-chamber spiral cochlear model provides a more accurate representation of inner ear mechanics. Because we also included the vestibular system which accounts for vestibulo-cochlear interactions, we believe that our models may account for confounding factors that less geometrically accurate models may not detect. These details give three-chambered models of the cochlea the capacity to exhibit a more realistic sensitivity to changing states of the inner ear. This makes them more widely applicable to further research. For example, the chinchilla model is capable of being attached to a model of the chinchilla middle and outer ear [130]. The middle ear transfer function in various scenarios could be recorded to aid in clinical diagnosis of scarification of tissues like the stapedial annular ligament and middle ear tissues.

In the future, a series of models derived from different species will continue to be developed in our lab to enhance inner ear implantable device design and evaluation of residual hearing and balance. With the addition of the nervous system, the models discussed in this work will be capable of simulating electrical and mechanical stimuli. Simulations in different species will assist electrode design at various stages (e.g. initial design in rodents, further optimization in primates, and clinical trials in humans).

Several models have focused on the vestibular system for the purpose of examining balance function and the interactions between the cochlea and vestibular system [113]. Most models have isolated the vestibular system for analysis and typically exclude the saccule. One such model was used to simulate the caloric test, used to quantify the vestibular signal as a result of irrigation of the ear canal

with hot and/or cold fluid. Caloric tests in clinical use quantify the vestibular signify using the vestibulo-ocular reflex, however in this model cupula deflection was the primary result. This model used the diaphragmatic model of the cupulae, where the cupulae span the entirety of the ampullae and are attached at to the membranous labyrinth at all sides. This model provided a precedent for the diphragmatic model of the cupulae. It also quantified the density changes of the endolymph in the utricle and SCC's, a valuable step in the understanding of the more intricate mechanics of the caloric test. A model created in our lab using μCT imaging as its data source included the entirety of the cochlea and vestibular system, though the fluid volume of the scala media was shrunk and the BM was not varied in width or thickness. Cupula motion as a result of OWM vibrations and BM displacement as a result of cupula motion were both analyzed. This model provided a better understanding of the interrelation between the cochlea and vestibular system, finding that their was a significant impact of the actions of one to the other [75]. This model was a good starting point for subsequent FE models in our lab given its anatomical accuracy. A similar model isolating the utricle and SCC's used experimental data in human subjects and compared cupula deflected as a function of angular acceleration of the head [136]. This is a test which could easily be conducted with the models described in this work.

Vestibular implants are a valuable new technology that are seeing many positive results in clinical trials in improving balance function [109] However, current spread remains an issue; stimulation of one cupula often stimulates another cupula leading to sensation of rotational acceleration in the wrong direction. A vestibular implant electrode could be added from medical imaging of an implanted unit to examine its effect on residual balance. Nervous tissues are clearly defined in the chinchilla and

rhesus μMRI scans presented here and have already been isolated in both models. Electrodes could be optimized with our finite element models to inform design of new electrode shapes and positions which minimize current spread of vestibular implants to surrounding nerves. A similar model to what we propose has been developed at Johns Hopkins using small spherical electrodes; we believe that the complex anatomy in our model coupled with a detailed model of the vestibular implant electrodes could lead to results which are more applicable to optimization of the electrodes [41].

By creating two FE models, one of the chinchilla inner ear and one of the rhesus inner ear, this work demonstrated the power of FE modeling in biomechanics by examining the effect of CI surgery on residual mechanical hearing function. A thorough procedure to generate such models was demonstrated, which is applicable to acoustic analysis of most any biological structure. The chinchilla model found that, absent cochlear trauma and post-implantation ossification, CI surgery can have a minimal effect on the mechanics of the inner ear. Tuning of the rhesus model through the phenomenological method is ongoing, however initial results are promising. These models will have direct clinical applications in the design of CI electrodes and surgical procedures for CI surgery. The flexibility of these models gives them broad applications in studying the inner ear with minimal man-hours compared to In Vivo animal testing, in addition to reducing cost and ethical issues associated with animal testing. Future mechanical applications include the study of ossification of inner and middle ear tissues, vestibulo-cochlear interaction, and the response of the vestibular sensory organs to acceleration of the head. These models also be modified to improve electrical stimulation of the spiral ganglion in the cochlea, and the design of vestibular implant electrodes to reduce current spread.

Overall, these models will be valuable tools in the field of cochlear mechanics for future studies.

6 Bibliography

[1] Harlow W. Ades and Hans Engström. *Anatomy of the Inner Ear*, pages 125–158. Springer Berlin Heidelberg, Berlin, Heidelberg, 1974.

[2] Yuri Agrawal, Bryan K. Ward, and Lloyd B. Minor. Vestibular dysfunction: Prevalence, impact and need for targeted treatment. *Journal of Vestibular Research*, 23(3):113–117, September 2013.

[3] Aysha Akhtar. The flaws and human harms of animal experimentation. *Cambridge Quarterly of Healthcare Ethics*, 24(4):407–419, September 2015.

[4] James R. Anderson and Arnold S. Chamove. Self-aggression and social aggression in laboratory-reared macaques. *Journal of Abnormal Psychology*, 89(4):539–550, 1980.

[5] Ansys Inc., Canonsburg, PA. Ansys, release 19.2, 2019.

[6] B. Areias, M.P.L. Parente, F. Gentil, and R.M. Natal Jorge. Finite element modelling of the surgical procedure for placement of a straight electrode array: Mechanical and clinical consequences. *Journal of Biomechanics*, 129:110812, December 2021.

[7] Thomas J. Balkany, Sarah S. Connell, Annelle V. Hodges, Stacy L. Payne, Fred F. Telischi, Adrien A. Eshraghi, Simon I. Angeli, Ross Germani, Sarah Messiah, and Kristopher L. Arheart. Conservation of residual acoustic hearing after cochlear implantation. *Otology & Neurotology*, 27(8):1083–1088, December 2006.

[8] Robert W. Baloh. Vestibular system. *Encyclopedia of the Neurological Sciences*, 4:661–671, 2003.

[9] Felix Bloch. Nuclear induction. *Physical review*, 70(7-8):460, 1946.

[10] B.A. Bohne and C.D. Carr. Location of structurally similar areas in chinchilla cochleas of different lengths. *The Journal of the Acoustical Society of America*, 66:411–414, 1979.

[11] Barbara A Bohne, Mary M Gruner, and Gary W Harding. Morphological correlates of aging in the chinchilla cochlea. *Hearing research*, 48(1-2):79–91, 1990.

[12] F Böhnke and W Arnold. 3d-finite element model of the human cochlea including fluid-structure couplings. *ORL J. Otorhinolaryngol. Relat. Spec.*, 61(5):305–310, September 1999.

[13] Frank Böhnke and Wolfgang Arnold. 3d-finite element modelof the human cochlea including fluid-structure couplings. *ORL*, 61(5):305–310, 1999.

[14] Frank Böhnke and Wolfgang Arnold. Bone conduction in a three-dimensional model of the cochlea. *ORL*, 68(6):393–396, 2006.

[15] Patrick J Bolan, Essa Yacoub, Michael Garwood, Kamil Ugurbil, and Noam Harel. In vivo micro-MRI of intracortical neurovasculature. *Neuroimage*, 32(1):62–69, August 2006.

[16] Annamaria A Bottini and Thomas Hartung. Food for thought... on the economics of animal testing. *ALTEX*, 26(1):3–16, 2009.

[17] J.J. Bradshaw, M.A. Brown, S. Jiang, and R.Z. Gan. 3d finite element model of human ear with 3-chamber spiral cochlea for blast wave transmission from the ear canal to cochlea. *Annals of biomedical engineering*, 2021.

[18] I.A. Bruce and I. Todt. Hearing preservation cochlear implant surgery. *Advances in Oto-Rhino-Laryngology*, page 66–73, 2018.

[19] John F. Brugge and Matthew A. Howard. Hearing. In *Encyclopedia of the Human Brain*, pages 429–448. Elsevier, 2002.

[20] D M Bruss and J A Shohet. *Neuroanatomy, Ear. In StatPearls*. StatPearls Publishing, 2022.

[21] Jane A. Burton, Michelle D. Valero, Troy A. Hackett, and Ramnarayan Ramachandran. The use of nonhuman primates in studies of noise injury and treatment. *The Journal of the Acoustical Society of America*, 146(5):3770–3789, November 2019.

[22] C Cai, H Zheng, MS Khan, and KC Hung. Modeling of material damping properties in ansys. In *CADFEM users' meeting & ANSYS conference*, pages 9–11, 2002.

[23] Kenneth L. Chiou, Michael J. Montague, Elisabeth A. Goldman, Marina M. Watowich, Sierra N. Sams, Jeff Song, Julie E. Horvath, Kirstin N. Sterner, Angelina V. Ruiz-Lambides, Melween I. Martínez, James P. Higham, Lauren J. N. Brent, Michael L. Platt, and Noah Snyder-Mackler. Rhesus macaques as a tractable physiological model of human ageing. *Philosophical Transactions of the Royal Society B: Biological Sciences*, 375(1811):20190612, September 2020.

[24] Indrajit Chowdhury and Shambhu P Dasgupta. Computation of rayleigh damping coefficients for large systems. *The Electronic Journal of Geotechnical Engineering*, 8(0):1–11, 2003.

[25] Mark N. Coleman. What do primates hear? a meta-analysis of all known nonhuman primate behavioral audiograms. *International Journal of Primatology*, 30(1):55–91, January 2009.

[26] I. S. Curthoys, C. H. Markham, and E. J. Curthoys. Semicircular duct and ampulla dimensions in cat, guinea pig and man. *Journal of Morphology*, 151:17–34, 01 1977.

[27] Ian S. Curthoys, Hilal Uzun-Coruhlu, Chris C. Wong, Allan S. Jones, and Andrew P. Bradshaw. The configuration and attachment of the utricular and saccular maculae to the temporal bone. new evidence from microtomography-ct studies of the membranous labyrinth. *Annals of the New York Academy of Sciences*, 1164:13–18, 05 2009.

[28] Chenkai Dai, Mohamed Lehar, Daniel Q. Sun, Lani Swarthout R.V.T., John P. Carey, Tim MacLachlan, Doug Brough, Hinrich Staecker, Alexandra M. Della Santina, Timothy E. Hullar, and Charles C. Della Santina. Rhesus cochlear and vestibular functions are preserved after inner ear injection of saline volume sufficient for gene therapy delivery. *Journal of the Association for Research in Otolaryngology*, 18(4):601–617, June 2017.

[29] A. Davis, C. M. McMahon, K. M. Pichora-Fuller, S. Russ, F. Lin, B. O. Olusanya, S. Chadha, and K. L. Tremblay. Aging and Hearing Health: The Life-course Approach. *Gerontologist*, 56 Suppl 2(Suppl 2):S256–267, Apr 2016.

[30] P. Dawes, R. Emsley, K. J. Cruickshanks, D. R. Moore, H. Fortnum, M. Edmondson-Jones, A. McCormack, and K. J. Munro. Hearing loss and cognition: the role of hearing AIDS, social isolation and depression. *PLoS One*, 10(3):e0119616, 2015.

[31] S.S. Desai, C. Zeh, and A. Lysakowski. Comparative morphology of rodent vestibular periphery. i. saccular and utricular maculae. *Journal of Neurophysiology*, 93:251–266, 2005.

[32] A. Dhanasingh. The rationale for flex (cochlear implant) electrode with varying array lengths. *World Journal of Otorhinolaryngology - Head and Neck Surgery*, 7:45–53, 2021.

[33] A. Dhanasingh and C. Jolly. An overview of cochlear implant electrode array designs. *Hearing Research*, 356:93–103, 2017.

[34] Anandhan Dhanasingh and Ingeborg Hochmair. Thirty years of translational research behind MED-EL. *Acta Otolaryngol.*, 141(sup1):i–cxcvi, March 2021.

[35] Sensory Functions & Disability and Rehabilitation teams. World report on hearing. Technical report, The World Health Organization, March 2021.

[36] Sonali K. Doke and Shashikant C. Dhawale. Alternatives to animal testing: A review. *Saudi Pharmaceutical Journal*, 23(3):223–229, 2015.

[37] Michael F. Dorman, Louise H. Loiselle, Sarah J. Cook, William A. Yost, and René H. Gifford. Sound source localization by normal-hearing listeners, hearing-impaired listeners and cochlear implant listeners. *Audiology and Neurotology*, 21(3):127–131, 2016.

[38] A. Fedorov, R. Beichel, J. Kalpathy-Cramer, J. Finet, J.-C. Fillion-Robin, S. Pujol, C. Bauer, D. Jennings, F. Fennessy, and M. Sonka. 3d slicer as an image computing platform for the quantitative imaging network. *Magnetic Resonance Imaging*, 30:1323–1341, 2012.

[39] Hope R. Ferdowsian and Nancy Beck. Ethical and scientific considerations regarding animal testing and research. *PLoS ONE*, 6(9):e24059, September 2011.

[40] Jacob Fish and Ted Belytschko. *A First Course in Finite Elements*. John Wiley & Sons, Inc., Hoboken, NJ, USA, 2007.

[41] Gene Y. Fridman and Charles C. Della Santina. Progress toward development of a multichannel vestibular prosthesis for treatment of bilateral vestibular deficiency. *The Anatomical Record: Advances in Integrative Anatomy and Evolutionary Biology*, 295(11):2010–2029, October 2012.

[42] Rong Z. Gan, Fan Yang, Xiangming Zhang, and Don Nakmali. Mechanical properties of stapedial annular ligament. *Medical Engineering & Physics*, 33(3):330–339, April 2011.

[43] R.Z. Gan, D. Nakmali, and X. Zhang. Dynamic properties of round window membrane in guinea pig otitis media model measured with electromagnetic stimulation. *Hearing Research*, 301:125–136, 2013.

[44] R.Z. Gan, B.P. Reeves, and X. Wang. Modeling of sound transmission from ear canal to cochlea. *Annals of Biomedical Engineering*, 35:2180–2195, 2007.

[45] K. Gautschi-Mills, K. Khoza-Shangase, and D. Pillay. Preservation of residual hearing after cochlear implant surgery: An exploration of residual hearing function in a group of recipients at cochlear implant units. *Brazilian Journal of Otorhinolaryngology*, 85:310–318, 2019.

[46] A. Geerardyn, M. Zhu, P. Wu, J. O'Malley, J.B. Nadol, M.C. Liberman, H.H. Nakajima, N. Verhaert, and A.M. Quesnel. Three-dimensional quantification of fibrosis and ossification after cochlear implantation via virtual re-sectioning: Potential implications for residual hearing. *Hearing Research*, 428:108681, 2023.

[47] A. E. Geers, J. G. Nicholas, and J. S. Moog. Estimating the Influence of Cochlear Implantation on Language Development in Children. *Audiol Med*, 5(4):262–273, 2007.

[48] R. H. Gifford, J. K. Shallop, and A. M. Peterson. Speech recognition materials and ceiling effects: considerations for cochlear implant programs. *Audiol Neurootol*, 13(3):193–205, 2008.

[49] René H. Gifford and G. Christopher Stecker. Binaural cue sensitivity in cochlear implant recipients with acoustic hearing preservation. *Hearing Research*, 390:107929, May 2020.

[50] J.M. Goldberg, R.A. Baird, and C. Fernández. Morphophysiological studies of the mammalian vestibular labyrinth. *Progress in Clinical and Biological Research*, 176:231–245, 1985.

[51] A. M. Goman and F. R. Lin. Prevalence of Hearing Loss by Severity in the United States. *Am J Public Health*, 106(10):1820–1822, Oct 2016.

[52] M. V. Goycoolea and L. Lundman. Round window membrane. structure function and permeability: a review. *Microscopy Research and Technique*, 36:201–211, 02 1997.

[53] D.D. Greenwood. A cochlear frequency-position function for several species–29 years later. *The Journal of the Acoustical Society of America*, 87:2592–2605, 1990.

[54] W K Gstoettner, O Adunka, P Franz, J Hamzavi, Jr, H Plenk, Jr, M Susani, W Baumgartner, and J Kiefer. Perimodiolar electrodes in cochlear implant surgery. *Acta Otolaryngol.*, 121(2):216–219, January 2001.

[55] Darcy L Hannibal, Eliza Bliss-Moreau, Jessica Vandeleest, Brenda McCowan, and John Capitanio. Laboratory rhesus macaque social housing and social changes: Implications for research. *Am. J. Primatol.*, 79(1):1–14, January 2017.

[56] R C Hawkes, G N Holland, W S Moore, and B S Worthington. Nuclear magnetic resonance (NMR) tomography of the brain: a preliminary clinical assessment with demonstration of pathology. *J. Comput. Assist. Tomogr.*, 4(5):577–586, October 1980.

[57] Shuman He, Holly F B Teagle, and Craig A Buchman. The electrically evoked compound action potential: From laboratory to clinic. *Front. Neurosci.*, 11:339, June 2017.

[58] Henry E Heffner and Rickye S Heffner. Hearing ranges of laboratory animals. *J. Am. Assoc. Lab. Anim. Sci.*, 46(1):20–22, January 2007.

[59] M. Hofmann, M. Meloche, and T.A. Zwolan. Health related quality of life in adolescent cochlear implant users. *Cochlear Implants International*, page 1–8, 2020.

[60] Carl Q. Howard and Benjamin S. Cazzolato. *Acoustic Analyses Using MATLAB and ANSYS ©*. Taylor & Francis Group, Boca Raton, 2015.

[61] Introduction to hypermesh, 2023.

[62] M. Igarashi, T. O-Uchi, H. Isago, and W. K. Wright. Utricular and saccular volumetry in human temporal bones. *Acta Oto-Laryngologica*, 95:75–80, 01 1983.

[63] Makoto Igarashi, Kozo Watanuki, Hideo Miyata, and Bobby R. Alford. Vestibular end organ mapping in the squirrel monkey. *Archives of Oto-Rhino-Laryngology*, 211:153–161, 1975.

[64] Hidehiro Ishikawa, Atsushi Niwa, Shinya Kato, Yuichiro Ii, Akihiro Shindo, Keita Matsuura, Yamato Nishiguchi, Asako Tamura, Akira Taniguchi, Masayuki Maeda, Yoshio Hashizume, and Hidekazu Tomimoto. Micro-MRI improves the accuracy of clinical diagnosis in cerebral small vessel disease. *Brain Commun.*, 3(2):fcab070, April 2021.

[65] M. Iso-Mustajärvi, S. Sipari, H. Löppönen, A. Dietz, and MeshMixer. Preservation of residual hearing after cochlear implant surgery with slim modiolar electrode. *European Archives of Oto-Rhino-Laryngology*, 2021(0128), 2019.

[66] C. Issing, U. Baumann, J. Pantel, and T. Stöver. Cochlear implant therapy improves the quality of life in older patients—a prospective evaluation study. *Otology & Neurotology*, 41:1214–1221, 2020.

[67] M.M. Iversen and R.D. Rabbitt. Wave mechanics of the vestibular semicircular canals. *Biophysical Journal*, 113:1133–1149, 2017.

[68] A Kawano, H L Seldon, and G M Clark. Computer-aided three-dimensional reconstruction in human cochlear maps: measurement of the lengths of organ of corti, outer wall, inner wall, and rosenthal's canal. *Ann. Otol. Rhinol. Laryngol.*, 105(9):701–709, September 1996.

[69] M.C. Ketterer, A. Aschendorff, S. Arndt, F. Hassepass, T. Wesarg, R. Laszig, and R. Beck. The influence of cochlear morphology on the final electrode array position. *European Archives of Oto-Rhino-Laryngology*, 275:385–394, 2017.

[70] H. Kingma and R. van de Berg. Chapter 1 - anatomy, physiology, and physics of the peripheral vestibular system. In Joseph M. Furman and Thomas Lempert, editors, *Neuro-Otology*, volume 137 of *Handbook of Clinical Neurology*, pages 1–16. Elsevier, 2016.

[71] D.M. Landsberger, M. Svrakic, J.T. Roland, and M. Svirsky. The relationship between insertion angles, default frequency allocations, and spiral ganglion place pitch in cochlear implants. *Ear & Hearing*, 36:207– 213, 2015.

[72] Thomas Lenarz. Cochlear implant - state of the art. *GMS Curr. Top. Otorhinolaryngol. Head Neck Surg.*, 16:Doc04, 2017.

[73] Hao Li, Gunesh P. Rajan, Jeremy Shaw, Seyed Alireza Rohani, Hanif M. Ladak, Sumit Agrawal, and Helge Rask-Andersen. A synchrotron and micro-CT study of the human endolymphatic duct system: Is meniere's disease caused by an acute endolymph backflow? *Frontiers in Surgery*, 8, May 2021.

[74] J. Liang, Z. Ke, P. V. Welch, R. Z. Gan, and C. Dai. A comprehensive finite element model for studying Cochlear-Vestibular interaction. *Comput Methods Biomech Biomed Engin*, 25(2):204–214, Feb 2022.

[75] J. Liang, Z. Ke, P.V. Welch, R.Z. Gan, and C. Dai. A comprehensive finite element model for studying cochlear-vestibular interaction. *Computer Methods in Biomechanics and Biomedical Engineering*, page 1–11, 2021.

[76] Manfred Liebsch, Barbara Grune, Andrea Seiler, Daniel Butzke, Michael Oelgeschläger, Ralph Pirow, Sarah Adler, Christian Riebeling, and Andreas Luch. Alternatives to animal testing: current status and future perspectives. *Archives of Toxicology*, 85(8):841–858, May 2011.

[77] D.J. Lim. Functional structure of the organ of corti: a review. *Hear Res*, 22:117–46, 1986.

[78] J. Lim, Y. Kim, and N. Kim. Mechanical effects of cochlear implants on residual hearing loss: A finite element analysis. *IEEE Transactions on Biomedical Engineering*, 67:3253–3261, 2020.

[79] W.W. Lo, D.L. Daniels, D.W. Chakeres, F.H. Linthicum, J.L. Ulmer, L.P. Mark, and J.D. Swartz. The endolymphatic duct and sac. *AJNR. American journal of neuroradiology*, 18:881–887, 1997.

[80] BON & LWE. Environmental noise guidelines for the european region. Technical report, The World Health Organization, Regional Office for Europe, January 2019.

[81] Andres Makarem, Jose N. Fayad, and Fred H. Linthicum. Endolymphatic pseudohydrops of the cochlear apex. *Otolaryngology–Head and Neck Surgery*, 143:269–273, 08 2010.

[82] C. H. McCollough, J. T. Bushberg, J. G. Fletcher, and L. J. Eckel. Answers to Common Questions About the Use and Safety of CT Scans. *Mayo Clin Proc*, 90(10):1380–1392, Oct 2015.

[83] Colette M. McKay. Applications of phenomenological loudness models to cochlear implants. *Frontiers in Psychology*, 11, 01 2021.

[84] T.R. McRackan, B.N. Hand, C.A. Velozo, and J.R. Dubno. Association of demographic and hearing-related factors with cochlear implant–related quality of life. *JAMA Otolaryngology–Head & Neck Surgery*, 145:422, 2019.

[85] MED-EL. Electrode arrays designed for atraumatic implantation providing superior hearing performance, 2018.

[86] Norimasa Morita, Shin Kariya, Armin Farajzadeh Deroee, Sebahattin Cureoglu, Shigenobu Nomiya, Rie Nomiya, Tamotsu Harada, and Michael M. Paparella. Membranous labyrinth volumes in normal ears and ménière disease: A three-dimensional reconstruction study. *The Laryngoscope*, 119:2216–2220, 10 2009.

[87] R.C. Naidu and D.C. Mountain. Longitudinal coupling in the basilar membrane. *Journal of the Association for Research in Otolaryngology*, 2:257–267, 2001.

[88] J. G. Nicholas and A. E. Geers. Will they catch up? The role of age at cochlear implantation in the spoken language development of children with severe to profound hearing loss. *J Speech Lang Hear Res*, 50(4):1048–1062, Aug 2007.

[89] Dominik Obrist. Flow phenomena in the inner ear. *Annual Review of Fluid Mechanics*, 51:487–510, 01 2019.

[90] Kenichi Odaka, Ichio Aoki, Junji Moriya, Kaoru Tateno, Hiroyuki Tadokoro, Jeff Kershaw, Tohru Minamino, Toshiaki Irie, Toshimitsu Fukumura, Issei Komuro, and Tsuneo Saga. In vivo tracking of transplanted mononuclear cells using manganese-enhanced magnetic resonance imaging (MEMRI). *PLoS One*, 6(10):e25487, October 2011.

[91] The National Institute of Deafness and Other Communication Disorders. Cochlear implants. Technical report, NIH, February 2016.

[92] H. Olze, A.J. Szczepek, H. Haupt, U. Förster, N. Zirke, S. Gräbel, and B. Mazurek. Cochlear implantation has a positive influence on quality of life, tinnitus, and psychological comorbidity. *The Laryngoscope*, 121:2220–2227, 2011.

[93] National Research Council (US) Committee on Disability Determination for Individuals with Hearing Impairments. *Hearing Loss: Determining Eligibility for Social Security Benefits*, chapter Basics of Sound, the Ear, and Hearing. National Academies Press (US), 2004.

[94] B.P. O'Connell, A. Cakir, J.B. Hunter, D.O. Francis, J.H. Noble, R.F. Labadie, G. Zuniga, B.M. Dawant, A. Rivas, and G.B. Wanna. Electrode location and angular insertion depth are predictors of audiologic outcomes in cochlear implantation. *Otology & Neurotology*, 37:1016–1023, 2016.

[95] Robia G Pautler and Scott E Fraser. The year(s) of the contrast agent - micro-MRI in the new millennium. *Curr. Opin. Immunol.*, 15(4):385–392, August 2003.

[96] Bryan E. Pfingst, Jim Laycock, Frank Flammino, Brenda Lonsbury-Martin, and Glen Martin. Pure tone thresholds for the rhesus monkey. *Hearing Research*, 1(1):43–47, 1978.

[97] S. Prodanovic, S.M. Gracewski, and J.-H. Nam. Power dissipation in the cochlea can enhance frequency selectivity. *Biophysical Journal*, 116:1362–1375, 2019.

[98] Edward M Purcell, Henry Cutler Torrey, and Robert V Pound. Resonance absorption by nuclear magnetic moments in a solid. *Physical review*, 69(1-2):37, 1946.

[99] R.D. Rabbitt, K.D. Breneman, C. King, A.M. Yamauchi, R. Boyle, and S.M. Highstein. Dynamic displacement of normal and detached semicircular canal cupula. *Journal of the Association for Research in Otolaryngology*, 10:497–509, 2009.

[100] R.D. Rabbitt, E.R. Damiano, and J.W. Grant. Biomechanics of the semicircular canals and otolith organs. *The Vestibular System*, page 153–201, 2004.

[101] Stefan Raufer, Cornelia Idoff, Aleksandrs Zosuls, Giacomo Marino, Nathan Blanke, Irving J. Bigio, Jennifer T. O'Malley, Barbara J. Burgess, Joseph B.

Nadol, John J. Guinan, and Hideko H. Nakajima. Anatomy of the human osseous spiral lamina and cochlear partition bridge: Relevance for cochlear partition motion. *Journal of the Association for Research in Otolaryngology*, 21(2):171–182, March 2020.

[102] Ansys, inc. theory reference manual, release 19.2.

[103] Liu-Jie Ren, Yi Yu, Yu-Heng Zhang, Xin-Dong Liu, Zeng-Jun Sun, Wen-Juan Yao, Tian-Yu Zhang, Cheng Wang, and Chen-Long Li. Three-dimensional finite element analysis on cochlear implantation electrode insertion. *Biomechanics and Modeling in Mechanobiology*, December 2022.

[104] Ulf Rosenhall. Vestibular macular mapping in man. *Annals of Otology, Rhinology & Laryngology*, 81:339–351, 06 1972.

[105] J.J. Rosowski, M.E. Ravicz, and J.E. Songer. Structures that contribute to middle-ear admittance in chinchilla. *Journal of Comparative Physiology A*, 192:1287–1311, 2006.

[106] I. Rotaru, C. Bujoreanu, A. Bele, M. Cazacu, and D. Olaru. Experimental testing on free vibration behaviour for silicone rubbers proposed within lumbar disc prosthesis. *Materials Science and Engineering: C*, 42:192–198, 2014.

[107] A.T. Roy, R.T. Penninger, M.S. Pearl, W. Wuerfel, P. Jiradejvong, C. Carver, A. Buechner, and C.J. Limb. Deeper cochlear removal. *Otology & Neurotology*, 37:146–151, 2016.

[108] P. Santi and P. Mancini. Cochlear anatomy and central auditory pathways. *Otolaryngology: Head and Neck Surgery*, 3:1–25, 2005.

[109] Charles Della C Santina, Americo A Migliaccio, Russell Hayden, Thuy-Ahn Melvin, Gene Y Fridman, Bryce Chiang, Natan S Davidovics, Chenkai Dai, John P Carey, Lloyd B Minor, Iee-Ching Anderson, HongJu Park, Sofia Lyford-Pike, and Shan Tang. Current and future management of bilateral loss of vestibular sensation — an update on the johns hopkins multichannel vestibular prosthesis project. *Cochlear Implants International*, 11(sup2):2–11, September 2010.

[110] Julia Sarant, David Harris, Peter Busby, Paul Maruff, Adrian Schembri, Richard Dowell, and Robert Briggs. The effect of cochlear implants on cognitive function in older adults: Initial baseline and 18-month follow up results for a prospective international longitudinal study. *Frontiers in Neuroscience*, 13, August 2019.

[111] Brian Schwarz and Mark Richardson. Proportional damping from experimental data. In Randall Allemang, James De Clerck, Christopher Niezrecki, and Alfred Wicks, editors, *Topics in Modal Analysis, Volume 7*, pages 179–186, New York, NY, 2014. Springer New York.

[112] Levent Sennaroğlu and Münir Demir Bajin. Classification and current management of inner ear malformations. *Balkan Med. J.*, 34(5):397–411, September 2017.

[113] S. Shen, Y. Liu, X. Sun, W. Zhao, Y. Su, S. Yu, and W. Liu. A biomechanical model of the inner ear: Numerical simulation of the caloric test. *The Scientific World Journal*, 2013:1–9, 2013.

[114] Takashi Shibata, Sumiko Matsumoto, Tetsuzo Agishi, and Teiko Nagano. Visualization of reissner membrane and the spiral ganglion in human fetal cochlea by micro-computed tomography. *American Journal of Otolaryngology*, 30(2):112–120, March 2009.

[115] F. Simon, J.-P. Guichard, R. Kania, J. Franc, P. Herman, and C. Hautefort. Saccular measurements in routine mri can predict hydrops in menière's disease. *European Archives of Oto-Rhino-Laryngology*, 274:4113–4120, 2017.

[116] F. W. Smith, J. M. Hutchison, J. R. Mallard, G. Johnson, T. W. Redpath, R. D. Selbie, A. Reid, and C. C. Smith. Oesophageal carcinoma demonstrated by whole-body nuclear magnetic resonance imaging. *Br. Med. J. (Clin. Res. Ed)*, 282(6263):510–512, February 1981.

[117] A.F.de Sousa, M.I.V. Couto, and A.C. Martinho-Carvalho. Quality of life and cochlear implant: Results in adults with postlingual hearing loss. *Brazilian Journal of Otorhinolaryngology*, 84:494–499, 2018.

[118] Timo Stöver and Thomas Lenarz. Biomaterials in cochlear implants. *GMS Curr. Top. Otorhinolaryngol. Head Neck Surg.*, 8:Doc10, 2009.

[119] S. Takano, H. Iguchi, H. Sakamoto, H. Yamane, and M. Anniko. Blockage pattern of longitudinal flow in meniere's disease. *Acta Oto-Laryngologica*, 133:692–698, 2013.

[120] Laila M Telmesani and Nithreen M Said. Electrically evoked compound action potential (ECAP) in cochlear implant children: Changes in auditory nerve response in first year of cochlear implant use. *Int. J. Pediatr. Otorhinolaryngol.*, 82:28–33, March 2016.

[121] Mathew Thomas, John J. Galvin, and Qian-Jie Fu. Importance of ipsilateral residual hearing for spatial hearing by bimodal cochlear implant users. *Scientific Reports*, 13(1), March 2023.

[122] M. Trevino, E. Lobarinas, A.C. Maulden, and M.G. Heinz. The chinchilla animal model for hearing science and noise-induced hearing loss. *The Journal of the Acoustical Society of America*, 146:3710–3732, 2019.

[123] Jeremy G Turner, Jennifer L Parrish, Larry F Hughes, Linda A Toth, and Donald M Caspary. Hearing in laboratory animals: strain differences and nonauditory effects of noise. *Comp. Med.*, 55(1):12–23, February 2005.

[124] M. Ulfendahl. Mechanical responses of the mammalian cochlea. *Progress in Neurobiology*, 53:331–380, 1997.

[125] M J van Gendt, J J Briaire, and J H M Frijns. Effect of neural adaptation and degeneration on pulse-train ECAPs: A model study. *Hear. Res.*, 377:167–178, June 2019.

[126] R.Häusler Vibert, M. Kompis, M. V, and D. Vestibular function in patients with cochlear implantation. *Acta Oto-Laryngologica*, 121:29–34, 2001.

[127] P.A. Vrettakos, S.P. Dear, and J.C. Saunders. Middle ear structure in the chinchilla: A quantitative study. *American Journal of Otolaryngology*, 9:58–67, 1988.

[128] Meredith Wadman. License of leading research chinchilla supplier permanently revoked, 2021. [Accessed 10-Apr-2023].

[129] M. Wang, J. Gao, and X. Wang. High-quality mesh generation for human hip based on ideal element size: Methods and evaluation. *Computer Assisted Surgery (Abingdon, England*, 22:212–220, 2017.

[130] X. Wang and R.Z. Gan. 3d finite element model of the chinchilla ear for characterizing middle ear functions. *Biomechanics and Modeling in Mechanobiology*, 15:1263–1277, 2016.

[131] G.B. Wanna, J.H. Noble, R.H. Gifford, M.S. Dietrich, A.D. Sweeney, D. Zhang, B.M. Dawant, A. Rivas, and R.F. Labadie. Implant patients. *Otology & Neurotology*, 36:1343–1348, 2015.

[132] Stefan Weder, Christofer Bester, Aaron Collins, Chanan Shaul, Robert J. Briggs, and Stephen O'Leary. Real time monitoring during cochlear implantation: Increasing the accuracy of predicting residual hearing outcomes. *Otology & Neurotology*, 42(8):e1030–e1036, April 2021.

[133] Katherine Wilson, Marette Ambler, Kate Hanvey, Marsha Jenkins, Dan Jiang, Justine Maggs, and Konstance Tzifa. Cochlear implant assessment and candidacy for children with partial hearing. *Cochlear Implants International*, 17(sup1):66–69, April 2016.

[134] Charles G. Wright and Peter S. Roland. Anatomy of the helicotrema and cochlear apex. *Cochlear Anatomy via Microdissection with Clinical Implications*, pages 27–43, 2018.

[135] Hung-Pin Wu, Chung-Ching Lin, Ting Chiu, Hong-Ping Chiou, Chu-Man Chang, and Chuan-Jen Hsu. Residual hearing preservation for cochlear implantation surgery. *Tzu Chi Medical Journal*, 33(4):359, 2021.

[136] X. Wu, S. Yu, W. Liu, and S. Shen. Numerical modeling and verification by nystagmus slow-phase velocity of the function of semicircular canals. *Biomechanics and Modeling in Mechanobiology*, 19:2343–2356, 2020.

[137] H. Yamane, K. Sunami, H. Iguchi, H. Sakamoto, T. Imoto, and H. Rask-Andersen. Assessment of meniere's disease from a radiological aspect – saccular otoconia as a cause of meniere's disease? *Acta Oto-Laryngologica*, 132:1054–1060, 2012.

[138] You-Cheng Yu, Tang-Chuan Wang, and Tzu-Ching Shih. Effects of age-related tympanic-membrane material properties on sound transmission in the middle ear in a three-dimensional finite-element model. *Computer Methods and Programs in Biomedicine*, 215:106619, March 2022.

[139] X. Zhang and R.Z. Gan. Dynamic properties of human round window membrane in auditory frequencies. *Medical engineering & physics*, 35:310–318, 2013.

[140] Xiangming Zhang and R.Z. Gan. A comprehensive model of human ear for analysis of implantable hearing devices. *IEEE Transactions on Biomedical Engineering*, 58:3024–3027, 2011.

[141] F. Zhao, V. K. Manchaiah, D. French, and S. M. Price. Music exposure and hearing disorders: an overview. *Int J Audiol*, 49(1):54–64, Jan 2010.

7 Appendix

EL	Endolymph	S	Saccule
PL	Perilymph	SM	Saccular Macula
BM	Basilar Membrane	U	Utricle
RM	Reissner's Membrane	UM	Utricular Macula
ML	Membranous Labyrinth	SCC	Semicircular Canal
RWM	Round Window Membrane	AC	Anterior Semicircular Canal
OWM	Oval Window Membrane	PC	Posterior Semicircular Canal
HT	Helicotrema	LC	Lateral Semicircular Canal
CI	Cochlear Implant	CAC	Cupula of the AC
CIE	Cochlear Implant Electrode	CPC	Cupula of the PC
CIS	Cochlear Implant Surgery	CLC	Cupula of the LC
RD	Reuniting Duct	OSL	Osseous Spiral Lamina
SV	Stria Vascularis	SAL	Stapedial Annular Ligament
VOR	Vestibulo-ocular Reflex		

Table 3: The abbreviations used for various terms in this work.